Excess methane in Greenland ice cores associated with high dust concentrations

James E. Lee[a,b,*], Jon S. Edwards[a], Jochen Schmitt[c], Hubertus Fischer[c], Michael Bock[c], Edward J. Brook[a]

[a] *College of Earth, Ocean, and Atmospheric Sciences, Oregon State University, Corvallis, OR 97331, USA*

[b] *Los Alamos National Laboratory, Earth Systems Observation, P.O. Box 1663 Los Alamos, NM 87545, USA*

[c] *Climate and Environmental Physics and Oeschger Centre for Climate Change Research, University of Bern, Switzerland.*

Abstract

Ice core records of atmospheric methane (CH_4) and its isotopic composition provide important information about biogeochemical cycles in the past. Interpreting these data requires that they faithfully record the composition of the atmosphere. In this study, we describe anomalies of up to 30-40 ppb CH_4 that are only observed in dust-rich (>∼60 ng Ca/g ice), glacial-period ice measured with standard melt-refreeze methods. The stable isotopic composition of CH_4 is also significantly affected. Results from the GISP2 and NEEM ice cores from Greenland show that excess CH_4 is either released or produced in the presence of liquid water in amounts which are highly correlated with the abundance of Ca^{2+} and mineral dust in the sample. Additional experiments show that excess CH_4 is unaffected by the addition of $HgCl_2$ (a microbial inhibitor) and is not related to ice core storage time. Dust concentrations in Antarctic ice cores are an order of magnitude lower than in Greenlandic ice cores and no excess CH_4 was observed in samples from the Antarctic WAIS Divide (WD) and South Pole (SPICE) ice cores. While the overall structure of the ice core atmospheric methane history is minimally impacted by excess CH_4, the impacts on the isotopic record and on inverse models used to reconstruct CH_4 sources are greater. We propose

*Corresponding author

Email address: jamesedlee@LANL.gov (James E. Lee)

three potential mechanisms to explain the presence of excess CH_4: (1) that CH_4 is adsorbed on dust particles prior to deposition on the ice sheet and is slowly desorbed during the melt-extraction step of sample analysis; (2) that dust acts as a micro-environment within the ice sheet for methanogenic extremophiles; or (3) that excess CH_4 is a product of abiotic degradation of organic compounds during the melt-extraction step of sample analysis.

Keywords: Methane, Greenland, Ice Cores, Isotope Geochemistry

1. Introduction

Ice cores from Greenland and Antarctica preserve the history of atmospheric methane (CH_4) and have been used to infer past changes in CH_4 sources (Thompson et al., 1993; Fischer et al., 2008; Bock et al., 2010b; Sowers, 2010; Rosen et al., 2014; Baumgartner et al., 2012, 2014; Rhodes et al., 2015; Bock et al., 2017). Natural sources of CH_4 are dominated by microbially produced CH_4 emitted from wetlands largely controlled by temperature and precipitation (Fung et al., 1991; Kirschke et al., 2013; Saunois et al., 2016). The ice core CH_4 record therefore provides important information, albeit indirect, about the history of terrestrial hydroclimate.

With traditional sampling techniques it has generally been assumed, with some exceptions, that the polar ice core CH_4 records are not affect by production of CH_4 within the ice (in situ production). Well-documented exceptions include samples altered by the presence of melt layers, which are known to cause elevated levels of CH_4 due to differential dissolution into liquid water (Campen et al., 2003; Mitchell et al., 2013; NEEM Community Members, 2013; Rhodes et al., 2016) or the entrainment of CH_4 and nutrient rich subglacial soils at the ice sheet bed (Souchez et al., 1995; Tung et al., 2005, 2006; NEEM Community Members, 2013). Anomalously high [CH_4] values were reported for several samples from the deep GISP2 ice core, but no explanation was provided for a potential cause (Brook et al., 1996). In contrast, elevated concentrations of other species (CO_2, N_2O, CH_3Cl) have been observed by a number of studies (Neftel et al., 1982; Anklin et al., 1995; Smith et al., 1997; Flückiger et al., 1999; Sowers, 2001; Stauffer et al., 2003; Saltzman et al., 2009) and linked to in situ processes.

Additional anomalies have been observed following the development of a continuous flow analysis technique for measuring ultra-high resolution records of [CH_4] Stowasser et al. (2012); Rhodes et al. (2013); Chappellaz et al.

(2013). Rhodes et al. (2013) observed infrequent, very brief large spikes in the concentration of CH_4 ($[CH_4]$, 20-100 cm depth range, 35-80 ppb magnitude) in the shallow NEEM-2011-S1 ice core which were confirmed by traditional analysis techniques. These spikes were associated with thin layers rich in carbon and nitrogen-containing impurities that may suggest biological in situ processes. Continuous records have also identified a mode of quasi-annual variability which affects the preservation of the atmospheric record and create the appearance of abrupt spikes in the record (Rhodes et al., 2013, 2015; Mitchell et al., 2015; Fourteau et al., 2017). This variability is related to variations in the depth at which bubbles lose off in the firn layer, which can vary due to seasonal differences in snow properties. At times of changing atmospheric composition these variation in close-off depth can create apparent fast variation in methane concentration that could resemble in situ production. The issue is discussed further below.

Here we present several lines of evidence which indicate that the $[CH_4]$ record preserved in some Greenlandic ice core samples is elevated above the atmospheric concentrations due to a process, different than those described above, which is closely related to the dust content of the samples. In Section 2 we discuss evidence from published records of $[CH_4]$ and show that excess CH_4 has also likely affected the isotopic composition of CH_4 in one record. In Section 3 we present $[CH_4]$ results following successive gas-extraction cycles which show that $[CH_4]$ in ice core samples increases during the melt-extraction step and allowing us to quantify the amount of CH_4 produced or released[1]. Additional experiments described in Section 3 provide information about the source of excess CH_4. In Section 4 we discuss potential mechanisms for explaining our results. Lastly, Sections 5 and 6 discuss the implications for interpreting atmospheric CH_4 records from ice cores and the viability of extremophiles in polar ice.

[1]Here we distinguish release from production, with the latter referring to the chemical or biological reaction resulting in the formation of new CH_4 in the flask during sample analysis while release refers to CH_4 which was already present in the ice sample but was previously in state preventing from exchange into the flask headspace.

2. Evidence for excess CH_4 in existing records

2.1. Discrepancies between ice core records

$[CH_4]$ is well sampled over the last glacial cycle from many Greenlandic ice cores (Chappellaz et al., 1993, 2013; Brook et al., 1996, 2000; Dällenbach et al., 2000; Blunier and Brook, 2001; Flückiger et al., 2004; Grachev et al., 2007; Baumgartner et al., 2014; Rosen et al., 2014). Dramatic, rapid fluctuations in atmospheric concentration ($[CH_4]$) are associated with Dansgaard-Oeschger events (DO-events) with high concentration associated with northern hemisphere warm periods (interstadials) and low concentrations during stadial (cold) conditions. These records were typically measured with a melt-extraction technique, where discrete samples are melted to liberate the entrapped air providing a single $[CH_4]$ value for each sample (Chappellaz et al., 1993; Flückiger et al., 2002; Blunier et al., 1993; Brook et al., 2000; Mitchell et al., 2011). Specific details of the process vary between laboratories, details regarding the technique used at Oregon State University (OSU) are described in Sect. 3 and Appendix B. Measurement uncertainty for individual discrete measurements (1-σ) considered in this manuscript is between 5-15 ppb (Baumgartner et al., 2014; Flückiger et al., 2004; Brook et al., 2000).

A number of records from Antarctica also exist (EPICA Community Members, 2006; Schilt et al., 2010; Loulergue et al., 2008; Buiron et al., 2012); the most detailed is a continuous flow analysis (CFA) record from the WAIS Divide ice core covering the time period from 9.8 to 67.8 ka (Rhodes et al., 2015). CFA involves the gradual melting of long, thin prismatic sticks of the core on a heated funnel-like melt head which produces a stream of water and bubbles for analysis (Stowasser et al., 2012; Rhodes et al., 2013; Chappellaz et al., 2013). Unlike in discrete sampling, the sticks can be stacked to avoid gaps in the record. This continuous technique was also used for the NEEM ice core from North Greenlandic although the NEEM record is only continuous for $\sim$30 cm sections from every 55 cm long melter sample (Stowasser et al., 2012; Chappellaz et al., 2013; Rhodes et al., 2017).

Ice cores contain a smoothed record of the local composition of the atmosphere. Due to the fast mixing of air between hemispheres (approximately 1 year) relative to the residence of CH_4 in the atmosphere (8-10 years), changes in the composition of one hemisphere will be quickly transferred to the other hemisphere. Ice cores from Antarctica and Greenland will record these changes as simultaneous events of unequal magnitudes. This is confirmed by comparing the NEEM continuous record with the WAIS Divide

continuous record (Fig. 1c). Although the values of [CH_4] are observed to be higher in the NEEM continuous record due to the uneven geographic distribution of CH_4 sources, changes in concentration essentially synchronous between the hemispheres (Rhodes et al., 2017).

By comparing [CH_4] records we identify variations which are observed in one ice core but lack an analogue in the continuous records from the NEEM and WAIS Divide ice cores (Fig. 1, see Fig. A.1 for comparison of [CH_4] records on the gas age scale). In this figure the WAIS Divide record is chosen as a reference because it is independently calibrated and because few gaps exist in the data. As noted by Rhodes et al. (2017), centennial-scale variability is well replicated in the WAIS Divide and NEEM continuous data sets and lends to the credibility of the NEEM record (Fig. 1c). To aide visual comparison, the WAIS Divide [CH_4] record has been shifted in Fig. 1. While the NEEM continuous [CH_4] record would allow for a more direct comparison to discrete Greenlandic records, doing so would be circular because it was calibrated to the discrete [CH_4] records in a piecewise manner (Chappellaz et al., 2013).

The comparison of discrete records with the continuous records shows specific intervals of elevated methane concentrations in the discrete data sets. These discrepancies are especially visible in the NGRIP [CH_4] record $\sim$500 years prior to the onset of Dansgaard-Oeschger event-8 and 12 (39.5-40.0 ka and 48.0-48.5 ka, hatched boxes in Fig. 1). In both of these time periods concentrations in the NGRIP [CH_4] record increased by $\sim$30 ppb during notably stable periods in the continuous NEEM or WAIS Divide [CH_4] records (Chappellaz et al., 2013; Rhodes et al., 2015). These discrepancies are much larger than the 5.9 ppb measurement error of the NGRIP ice core (Baumgartner et al., 2014). Since samples for the NGRIP ice core were measured in random order and these periods consist of ten and seven measurements, respectively, these offsets are not likely to be related to instrumental artifacts. There are similar features in the GISP2 and GRIP records (Fig. 1b, c), although the chronological uncertainties and sample resolution of these records limit precise comparison to the NEEM and WAIS Divide records.

Other notable differences are observed during DO-10 and 11 (40.95-41.35 ka and 42.68-43.25 ka, respectively) and are again clearest in the NGRIP [CH_4] record (Fig. 1a). During DO-10, peaks at the onset and at the termination of the interstadial are observed in both the NEEM and WAIS Divide [CH_4] records with similar values at both peaks and a near constant offset between the records (Fig. 1c). In contrast, [CH_4] observed in the NGRIP

ice core tends to increase throughout the interstadial resulting in [CH_4] at the end of the interstadial being ∼40 ppb (±8.4 ppb) higher than at the beginning. A similar feature is observed during DO-11 when comparing the NGRIP and WAIS Divide records, however it is not possible to verify this feature because of a gap in the NEEM record at this time.

Elevated [CH_4] in normal ice was occasionally observed in previous studies, such as in the GISP2 record at 37.87 ka, 38.33 ka, and 47.27 ka (Brook et al., 1996) and in the shallow NEEM-2011-S1 ice core (Rhodes et al., 2013). With the recent ultra-high resolution [CH_4] records inconsistencies between ice cores are more clearly discerned. In general, we observe that in certain sections Greenlandic ice samples measured with a discrete wet extraction technique appear to be elevated in comparison to the records measured with a continuous technique. These elevated sections are much more extensive than the in situ-derived spikes observed in Rhodes et al. (2013) and have not counterparts in the continuous WAIS Divide or NEEM records. This implies that additional CH_4 is related to the measurement technique, as discussed in detail below. Although in both cases the sample is melted, with CFA the gas is quickly separated from the liquid stream (2-3 minutes) providing only a short time period for the release or production of CH_4 in comparison to discrete measurements (typically 15-30 minutes). Additionally the discrete method usually, but not always, involves refreezing the sample after gas extraction which could influence how much CH_4 remains trapped in the sample water/ice.

2.2. Links between proxies of dust and excess CH_4

Discrete [CH_4] measurements from Greenlandic ice samples tend to be elevated relative to the continuous records when the ice age of the sample corresponds to a stadial period when Ca^{2+} concentrations are high (gray bars in Fig. 1). Ca^{2+} is commonly assumed to be a proxy for continental dust (Steffensen, 1997) but covaries with the concentration of many other impurities (Mayewski et al., 1997; Schüpbach et al., 2018). Variations in its abundance are recorded in ice cores throughout Greenland. The ice cores considered here have similar concentrations of Ca^{2+} (Rasmussen et al., 2014). Air in an ice core sample is offset in depth from ice of the same age because bubble close off only happens at a depth of 50-100 m within the firn (Schwander and Stauffer, 1984). To account for this offset we have translated the [CH_4] measurements on to the GICC05 ice age scale (Rasmussen et al.,

2014) to allow direct comparison to variations of Ca^{2+} (Fig. 1e, Rasmussen et al. 2014).

As shown in hatched boxes in Fig. 1, a 30 ppb increase in [CH_4] is observed prior to both DO-8 and DO-12 in the NGRIP [CH_4] record at the same depth where Ca^{2+} increases from ∼60 ng/g to >600 ng/g. Concentrations of CH_4 remain elevated as long as Ca^{2+} concentrations are high and then decrease by 10-20 ppb when Ca^{2+} returns to interstadial values at 38 and 47 ka (ice age). Several samples with elevated [CH_4] values were also observed in the GISP2 and GRIP records prior to DO-8 and DO-12 (as expressed in [CH_4]) and correspond to dust-rich ice in those ice cores (Fig. 1b, d). The link between Ca^{2+} and elevated [CH_4] is also evident as a small minimum in both the NGRIP and GISP2 [CH_4] records during DO-9 (∼40 ka ice age), a brief period of low dust concentration between two stadials. Elevated values may also exist during other dusty periods but the identification is complicated by the coincidence of abrupt changes of both [CH_4] and Ca^{2+} (such as at 35.5 and 36.5 ka ice age), by age uncertainties of the [CH_4] records (such as at 40-41 ka), or because the low-resolution of older records resulted in no stadial ice being measured for [CH_4] (as is the case for the GISP2 and GRIP ice cores at 44.6 and 49.3 ka).

2.3. Isotope anomalies associated with excess CH_4

Atmospheric CH_4 is isotopically heavier (higher isotopic ratios of $^{13}C/^{12}C$ and $^{2}H/^{1}H$) than the globally integrated CH_4 source due to isotope fractionation in atmospheric sink reactions. This is particularly true of $\delta D(CH_4)$, for which the atmosphere is heavier than all significant sources and the isotopic difference of the atmosphere from the globally integrated source composition is ∼200‰ (Quay et al., 1999; Whiticar and Schaefer, 2007). For this reason, it is likely that any contribution from excess CH_4, which would not be subject to atmospheric sink processes, will significantly lower the measured isotopic value.

$\delta D(CH_4)$ has been measured for the time period 33.68-40.99 ka gas-age (34.9-41.9 ka ice-age) from samples from the NGRIP ice core (Bock et al., 2010b) using a wet extraction technique (Bock et al., 2010a). Unlike the melt-refreeze techniques used to measure [CH_4], the technique used by Bock et al. (2010a,b) does not involve refreezing the sample. Figure 2 shows records of [CH_4] and $\delta D(CH_4)$ plotted on the NGRIP GICC05 ice age scale for direct comparison to the NGRIP Ca^{2+} record (Rasmussen et al., 2014). Several large negative isotopic excursions were observed that were difficult to explain

because of the lack of a correspondingly large change in concentration or a mechanism which would cause a switching between different source types. The largest feature is a 16‰ depletion which begins at 39.74 ka (2106 m, 40.0 ka ice-age), ∼500 years prior to the onset of DO-8 as observed in the $[CH_4]$ record (Fig. 2b) and is co-registered in depth with a >10x increase in Ca^{2+} and the late-stadial rise of 30 ppb in $[CH_4]$ discussed in Sect. 2.1. Two other well sampled excursions, both depletions of >6‰ (35.3-36.6 ka and 40.4-41.1 ka), are also associated with dust peaks. The one other well sampled excursion noted by Bock et al. (2010b) (2048-2069 m, 36.5-37.0 ka gas-age, 37.5-38.1 ka ice-age) is not associated with high dust concentrations but is also not associated with significant variability of $[CH_4]$. Since these samples were not refrozen prior to the gas extraction step, evidence of excess CH_4 in this record implies that its release/production is not related to the refreezing of the sample.

Ice samples from the GISP2 ice core were also measured for $\delta D(CH_4)$ using a wet extraction technique (Sowers, 2006). A seven-sample subset of these overlaps in age with the $\delta D(CH_4)$ measurements from NGRIP. This subset reveals a ∼16‰ depletion concurrent with the abrupt increase in $[CH_4]$ during the onset of DO-8. Although the magnitude of this depletion is similar to the one seen in the NGRIP ice core, the depletions differ in their phasing with respect to changes in $[CH_4]$ and the depletion in the GISP2 ice core is not associated with an increase in dust concentration. The GISP2 $\delta D(CH_4)$ record is difficult to interpret: first, because it only encompasses a brief time period (39.05 to 39.60 ka, ice age) during which $[CH_4]$ increased abruptly; second, because there is a large offset between the GISP2 and NGRIP $\delta D(CH_4)$ records (Umezawa et al., 2018); and, third, because the GISP2 record exhibited large sample-to-sample variability during the more detailed deglacial section (Sowers, 2006).

3. Experimental investigation of excess CH_4

3.1. Measurement of release/production of CH_4 in the OSU analytical system

Excess CH_4 was measured at Oregon State University (OSU) with a multiple refreeze process. First, $[CH_4]$ was measured following the typical procedure described by Grachev et al. (2009) and Mitchell et al. (2013) with updates described in Lee et al. (2018). Briefly, 32-65 g ice samples are placed in glass flasks which are then attached to a high vacuum line. Flasks are immersed in a chilled ethanol bath set to -70° C to keep the samples frozen.

After laboratory air has been evacuated, the flasks are sealed from the vacuum and the samples are melted in a hot water bath, initially 50° C (±1° C), for 30 minutes to liberate the air into the flask headspace. Samples typically require 15-25 minutes to finish melting, depending on the size of samples and whether the ice is bubbly or clathrated. The flasks are then re-immersed in the cold ethanol bath. Once the melt water is completely refrozen, air from the headspace is expanded into a sample loop in a gas chromatograph (GC). Pressure in the sample loop is recorded and the air is injected into the GC system for $[CH_4]$ measurement. Expansion air in the flask headspace into the GC system is repeated four times for four individual readings during this measurement set. Absolute uncertainty of $[CH_4]$ values for measurements presented here is 1.8 ppb (pooled standard deviation of depths sampled multiple times, n=96 sample depths).

Following the typical procedure we begin additional analysis to quantify excess CH_4. The refrozen ice is left in the glass vessels with the remaining sample air (about 30%) after the GC measurement. The melt-refreeze extraction step is repeated and then we re-measure the $[CH_4]$ by expanding air in the headspace into the GC either 2 or 4 times. The difference between the average of the first and second set of measurements is referred to as ΔCH_4. Uncertainty of ΔCH_4 was determined to be 4.4 ppb (pooled standard deviation of replicated sample depths). Interpretation of ΔCH_4 is discussed below.

This procedure was applied to ice samples from several ice cores with very different impurity compositions and concentrations (data available `https://www.ncdc.noaa.gov/paleo/study/27610`). Most of our samples are from the Greenlandic GISP2 ice core (154 samples) and the Antarctic WAIS Divide ice core (82 samples). We also include measurements from the NEEM ice core from Greenland (40 samples) and the Antarctic South Pole ice core (SPICE ice core, 19 samples) as well as measurements made on bubble free ice (BFI, 62 samples) that we produce using ultra-pure deionized water and which we interspersed with our other samples. Temporally, our samples include overlapping measurements from the WAIS Divide, GISP2, and NEEM ice cores dated between 42 - 50 ka and five more samples from the GISP2 ice core from 72-75 ka (Sect. 3.4). Samples from the SPICE ice core are from various ages during the last glacial cycle.

Figures 3a, b and 4a, b show results from the first and second set of $[CH_4]$ measurements and of ΔCH_4 for samples from the GISP2 and NEEM ice cores. ΔCH_4 is observed to be positive for almost every sample, including

BFI samples. Small increases in [CH_4] are expected due the higher solubility of CH_4 in comparison to N_2 and O_2 (the main components of air). This causes the melt water to be slightly enriched in CH_4 with respect air in the headspace. The refreezing process does not perfectly expel all gases from the melt-water. During the second melt-extraction step, this CH_4 degases from the melt-water due to the reduced gas pressure from GC measurements and causes [CH_4] in the headspace to increase. The quick refreezing of the ice sample is one way which the OSU measurement methodology varies from other laboratories (Chappellaz et al., 1997; Flückiger et al., 2004). The trapping of gas in the refrozen sample is referred to as the solubility effect and can explain ΔCH_4 values observed for samples with low-dust concentrations.

For GISP2 and NEEM samples, ΔCH_4 closely follows the quantity of Ca^{2+} in the sample (Fig. 3d and 4d). Although solubility of gases decrease with increasing concentration of ions, the large values of ΔCH_4 in samples with high concentrations of Ca^{2+} exceeds what is possible by solubility effects alone (i.e. more CH_4 is degassed than could be trapped in the ice). To quantify the amount of additional CH_4 (excess CH_4) the effects of solubility must be removed. Another important observation is that our approach is only feasible because the release/production of excess CH_4 is slow relative to the melt phase of extraction, i.e. the release/production of excess CH_4 is not complete during the first extraction and resumes during sequential melt-extractions. This implies that ΔCH_4 is sensitive to the duration of the melt-refreeze extraction and necessitates consistent extraction conditions.

3.2. Quantifying excess CH_4 from measurements

To quantify the total amount of excess CH_4 generated we need to constrain the quantity that remains in the refrozen meltwater at the end of the second melt-refreeze step. This cannot be directly measured. Instead we estimate this value by determining the typical solubility effect for each ice core empirically based on samples with low-dust content and accounting for variations in [CH_4], total air content, sample mass, and for differences in the volume between sample flasks (Description of the methods used to determine solubility effects are provided in Appendix B). This allows us to estimate an expected ΔCH_4 for each sample. Excess CH_4 is then defined as difference between the measured ΔCH_4 and the expected value and is provided in units of moles of CH_4. The equations used to quantify the amount of excess CH_4 released/produced (n^*_{xs}) are provided in Appendix C.

Figures 3c and 4c show n^*_{xs} versus depth for the GISP2 and NEEM ice cores, respectively. Values of n^*_{xs} range from 0 to ∼6 picomoles and are closely related to the measured value ΔCH_4. Pooled standard deviation of replicate measurements of n^*_{xs} is 0.4 picomoles and is independent of n^*_{xs} and from which core it was determined. Values of n^*_{xs} from the WAIS Divide or SPICE ice core samples were not statistically different than 0. Those results were not plotted but are included in the Supplementary Material. The largest value of n^*_{xs} was observed in a dusty sample from the NEEM ice core (Fig. 4c) and would have been equivalent to a 9% (40 ppb) increase in $[CH_4]$ if released/produced during the first melt extraction. Although some differences exist, the ∼30-40 ppb impact of excess CH_4 on GISP2 and NEEM $[CH_4]$ measurements preceding DO-12 is similar to that inferred for the GRIP and NGRIP $[CH_4]$ record for the same time period (Sect. 2.1). Since both the GRIP and NGRIP $[CH_4]$ measurements were made with a similar melt-extraction technique to that used at OSU (Chappellaz et al., 1997; Blunier et al., 1998; Flückiger et al., 2002; Baumgartner et al., 2014), these records are also likely affected by excess CH_4.

In both the GISP2 and NEEM ice core results, n^*_{xs} is highly correlated with the concentration of chemical impurities (Fig. 5, Table 1). Elements commonly associated with continental dust (Ca^{2+}, Mg^{2+}, and K^+) show the highest correlation to the GISP2 results (R^2=0.78 with Ca^{2+}, n=108 samples) while ammonium and nitrate (common nutrients) have a significantly weaker correlation (R^2=0.20 and R^2=0.33, respectively). Strong relationships are also observed between the NEEM n^*_{xs} measurements with both Ca^{2+} and particle counts from the NEEM ice core (R^2=0.64 and R^2=0.59, respectively, n=32 samples).

A regression between Ca^{2+} concentration and n^*_{xs} for the GISP2 results indicates that ∼5 ± 0.5 μmol of CH_4 (95% CI) are produced per mole of Ca^{2+} in the sample (150 ng CH_4/g Ca^{2+}, Fig 5). We emphasize that this is simply the observed statistical association and it does not imply a stoichiometric relationship. Since the process which releases/produces excess CH_4 is not allowed to continue to completion and different laboratories melt their samples at different temperatures and for different lengths of time, this ratio is probably specific to the OSU system and measurement procedure. Regardless, we find that the relationship is consistent for GISP2 samples from both the 42-50 ka period as well as the 5 samples from 72-75 ka (Fig. 5). We attribute the lack of excess CH_4 in WAIS Divide and SPICE ice core samples to the much lower dust concentrations (typically an order of magnitude less)

and possibly to differences in dust mineralogy.

An ad hoc correction to the measured concentration can be made by subtracting n^*_{xs} from the first set of measurements (which followed the first melt-extraction). While n^*_{xs} represents the quantity of CH_4 released/produced during the second extraction, differences in melting conditions between the first and second extractions make it difficult to assess whether this is an overestimate or underestimate of CH_4 released/produced during the first extraction. For simplicity we assume an equal addition of CH_4 during each of these steps.

In Fig. 6, corrected [CH_4] records from the GISP2 and NEEM ice cores are plotted with the WAIS Divide and NEEM continuous records. The 30 ppb pre-DO-12 increase in [CH_4], well captured in the uncorrected measurements, is not present in the corrected GISP2 record. Better agreement in absolute concentrations between the NEEM discrete measurements and GISP2 measurements is observed after the correction. Agreement of multi-decadal to multi-centennial scale variability, particularly during DO-12, is also observed between the corrected records of the NEEM and GISP2 ice cores and the WAIS Divide and NEEM continuous records but not in the uncorrected discrete records. While these observations lead us to believe that our ad hoc correction has improved our interpretation of atmospheric [CH_4], more work is needed to develop a quantitative and more precise correction for [CH_4] measurements. Such a correction will need to be verified by measurements of [CH_4] unaffected by excess CH_4 from dusty Greenlandic ice samples.

3.3. An estimate of the $\delta D(CH_4)$ signature of excess CH_4

The effect of excess CH_4 on $\delta D(CH_4)$ can be assessed using the NGRIP [CH_4] (Baumgartner et al., 2014) and $\delta D(CH_4)$ records (Bock et al., 2010b). Both records were measured with a melt-extraction technique (Bock et al., 2010a; Flückiger et al., 2004; Baumgartner et al., 2014). Here, we assume that the ice core sample represents a two-component mixture with end members of atmospheric air and excess CH_4 (represented by Eqn. 1).

$$\delta D(CH_4)_{model} = (1 - f_{xs}) \cdot \delta D(CH_4)_{atm} + f_{xs} \cdot \delta D(CH_4)_{xs} \quad (1)$$

In this model, the measured stable isotopic composition of CH_4 is dependent on the isotopic compositions of the atmospheric component ($\delta D(CH_4)_{atm}$), the excess component ($\delta D(CH_4)_{xs}$), and the relative contribution of excess CH_4 ($f_{xs} = [CH_4]_{xs}/[CH_4]_{measured}$).

In both the NEEM and WAIS Divide continuous [CH_4] records, stable [CH_4] was observed for the ∼1000 year period preceding DO-8 (Chappellaz et al., 2013; Rhodes et al., 2015). We use this time period to estimate $[CH_4]_{xs}$, assuming that atmospheric [CH_4] was constant and comparing the difference of the NGRIP [CH_4] and the atmospheric value to the concentration of Ca^{+2}. The resulting relationship of Ca^{2+} is: $[CH_4]_{xs}$ (ppb) =0.091·(Ca^{2+} (ng/g) - 43). Equation 1 can then be rearranged:

$$\delta D(CH_4)_{model} = \delta D(CH_4)_{atm} + (\delta D(CH_4)_{xs} - \delta D(CH_4)_{atm}) \cdot \frac{0.091 \cdot (Ca^{2+} - 43)}{[CH_4]_{measured}} \quad (2)$$

We solve for $\delta D(CH_4)_{xs}$ using a best-fit two-sided regression comparing $\delta D(CH_4)_{model}$ to the NGRIP $\delta D(CH_4)$ record ($\delta D(CH_4)_{measured}$) following the method of York et al. (2004) which accounts for errors in both variables. Weights for the fit are derived from measurement uncertainties of [CH_4], Ca^{2+} (constant 10%), and $\delta D(CH_4)_{measured}$ (constant 3.4‰) and the regression uncertainty between [CH_4] and Ca^{2+}. Best fit values were determined to be $\delta D(CH_4)_{xs}$=-293‰ (± 31‰ 95% CI, n=51, R^2=.53) and $\delta D(CH_4)_{atm}$=-82.2‰ (± 0.7‰ 95% CI). This provides a good fit to the NGRIP $\delta D(CH_4)$ record despite the assumption of a constant atmospheric history (Fig. 7).

3.4. Microbial inhibition experiment

As described in sections 3.1-3.3, our observations indicate that a previously unknown process either releases or produces CH_4 during the melt-refreeze extraction step of analysis. One possibility is that microbial production occurs when the sample is melted. Microbial methanogenesis favors anoxic conditions ([O_2]<0.5 mg·L^{-1}), a condition which is met during melting of our samples because of the small amount of air remaining in the sample flask after evacuating contemporary air. Under this hypothesis, production of CH_4 would scale with either the nutrient availability, cell abundance, or both.

We tested this possibility by inhibiting biologic activity with 25 μL of saturated mercuric chloride ($HgCl_2$) solution added to selected samples (54-58 g). This quantity of $HgCl_2$ is enough to inhibit microbial activity in samples of sea water of similar volume (Oxtoby et al., 2016). A control of each sample was also measured without $HgCl_2$. Samples used in this test

were from the GISP2 ice core and date between 72-75 ka which includes DO-20, a period of low dust concentrations ([Ca^{2+}]<35 ng·g^{-1}), and the succeeding dusty stadial interval ([Ca^{2+}]>350 ng·g^{-1}). These GISP2 samples were previously measured by Grachev et al. (2009) on an earlier version of the OSU system.

Figure 8 shows the results of this test. Despite the ∼10 years between when these samples were measured, our new measurements reproduce values from Grachev et al. (2009) well within measurement uncertainty (mean difference of 3.6 ppb ± 1.4 ppb, measurement uncertainty from Grachev et al. (2009) of 2 ppb, absolute uncertainty of new measurements of 2.4 ppb). There was no difference in [CH_4] between samples that had been poisoned with $HgCl_2$ and their replicate which had not, in either the first or second set of measured concentrations (Fig 8). The ratio of n^*_{xs} compared to the number of moles of Ca^{2+} in the samples was consistent with that observed in Sect. 3.2. This set of observations indicates that either microbes were tolerant of this concentration of $HgCl_2$, which seems unlikely, that CH_4 is produced abiotically, or that CH_4 was formed prior to the original analysis of the ice samples and released during sample processing.

4. Potential sources and pathways for excess CH_4

In section 2 and 3 we provide evidence for excess CH_4 and attempt to quantify the effect of excess CH_4 in ice core samples measured at OSU. To summarize our observations of excess CH_4 in Greenlandic ice core samples:

- Release/production of excess CH_4 occurs slowly (hours) when liquid water is present during the melt-extraction of air from the ice sample (Sect. 3.1 and 3.2). Excess CH_4 is observed whether or not the sample is refrozen after extraction.

- Elevated CH_4 values are not observed in measurements using a continuous technique which separates gases from the melted sample within minutes. This distinguishes excess CH_4 from the spikes observed by Rhodes et al. (2013).

- Release/production of excess CH_4 is not inhibited by the addition of $HgCl_2$ to the sample (Sect. 3.4).

- The amount of excess CH_4 released/produced during extraction is correlated with the amount of dust in the ice core sample (Sect. 2.2 and

3.2) and the relationship is the same for samples dated between ∼42-50 ka and ∼72-75 ka (Sect. 3.4).

- The amount of excess CH_4 released/produced is independent of the length of time the ice core has been stored since it was recovered (Sect. 3.4).

- Excess CH_4 was measured in samples from multiple Greenlandic ice cores (GISP2 and NEEM ice cores), but not in Antarctic ice core samples (WAIS Divide and SPICE) using the standard extraction time (Sect. 3.1 and 3.2). Analogous anomalies in $[CH_4]$ can be observed in the GRIP and NGRIP records (Blunier et al., 1998; Baumgartner et al., 2014) (Sect. 2.1).

- $\delta D(CH_4)_{xs}$ is estimated to be ∼-293‰ (± 31‰ 95% CI), which consistent with biogenically produced CH_4 (Sect. 3.3).

We now review several possible mechanisms which could lead to the addition of excess CH_4, and evaluate their viability.

4.1. Artifacts of drilling and storage

Artifacts may include any production or addition of CH_4 during or after the drilling of the ice core. This may include direct contamination, such as the closing of bubbles or cracks in the ice core after extraction from the ice sheet (Aydin et al., 2010) which can trap modern air with high $[CH_4]$ or contaminate the sample with drill fluid. As is the case with many types of artifacts, post-coring bubble or fracture close-off would not produce/release CH_4 during the second melt-refreeze extraction and therefore would not produce an excess signature as we have defined it. Additionally, it is unlikely that this sort of direct contamination would only affect records from Greenland and result in a close correlation with the dust content of the sample. We therefore find it unlikely that excess CH_4 is related to a direct contamination of the ice core.

Artifacts could also include indirect contamination, for example an unknown reaction involving drill fluid or the introduction of microbes to the ice core after the core was recovered. We do not expect that these processes are the cause of our measured excess CH_4 as samples are trimmed thoroughly so that any such contaminant is removed. Additionally, if post-coring production happens it must occur during the first few years after drilling based

on: (1) the good agreement between our measured [CH_4] values from GISP2 with older measurements (Grachev et al., 2009) and (2) the similar relationship between excess CH_4 and Ca^{2+} observed for the GISP2 ice core drilled in 1993 and the NEEM ice core which was drilled in 2011. All samples were measured between July 2016 and February 2017. Given the storage conditions (typically -30 to -50^o C) it seems unlikely that microbes could produce the observed excess CH_4 in the short time frame and that production would stop.

4.2. "In Vitro" production of CH_4

A special case of an artifact is the production of CH_4 under the specific conditions of the measurement procedure. We refer to the possibility of biologic or chemical production of CH_4 during the melt-extraction process as "in vitro" (in reference to the glass flasks used for CH_4 analysis). In vitro production matches many of the observations of excess CH_4 such as the production would occur in the presence of water, would be time dependent, and would potentially be nutrient or cell limited.

We believe microbial production in the flask is unlikely given that the addition of excess CH_4 was unhindered in the presence of $HgCl_2$ (Sect. 3.4) and that the negative $\delta D(H_2O)$ (typical values between -300 to -320‰, Jouzel et al. 2007) would likely result in an isotopically lighter signature than inferred for $\delta D(CH_4)_{xs}$ (Sect. 3.3). CH_4 can also be produced abiotically from organic carbon (Wang et al., 2017; Hurkuck et al., 2012), a pathway which would not be affected by $HgCl_2$. These mechanisms include UV irradiation (Fraser et al., 2015), heating (Jugold et al., 2012; Hurkuck et al., 2012), or the presence of reactive oxidating species to cleave organic molecules (Jugold et al., 2012). All of these studies involved soil samples and mechanisms that would require large quantities of organic carbon precursor. While similar conditions are not present during our experiments we cannot definitively rule out an abiotic mechanism.

4.3. Production related to surface melt events

Spikes in [CH_4] in ice cores have been found in the presence of refrozen surface melt layers (Campen et al., 2003; Mitchell et al., 2013; NEEM Community Members, 2013; Rhodes et al., 2016). These spikes can partially be explained by the higher solubility of CH_4 than the major air constituents. However, in some cases the measured [CH_4] exceeded what was expected from equilibrium solubility alone suggesting that surface melt promotes some other

in situ process which further enhances [CH_4] (Campen et al., 2003; NEEM Community Members, 2013; Schmitt et al., 2014; Rhodes et al., 2016). We do not believe that the elevated [CH_4] that we observe in the NEEM and GISP2 ice cores are related to the occurrence of melt layers for two reasons. First, the elevated [CH_4] values we measured occur only in ice that was deposited during cold stadial periods but not during warm interstadials when melt layers may be more frequent. Second, the mechanism would not explain the continued addition of CH_4 in sequential melt-refreeze cycles during sample processing.

However, production due to melt layer formation is similar to the process which releases/produces excess CH_4 described here in that the increase in [CH_4] appears to be related to the presence of liquid water, implying that the unknown process affecting melt layers could be similar to that affecting discretely measured samples. Interestingly, Campen et al. (2003) measured anomalies in [CH_4] with a dry extraction technique and the possibility of melt layers affecting these samples was excluded by measurements of noble gas ratios on co-registered depths. Without the presence of water during extraction the elevated values they observed were probably the result of a different process than that observed here.

4.4. Annual "trapping" signal

Mitchell et al. (2015) and Rhodes et al. (2013, 2016) observed a quasi-annual variability of [CH_4] preserved in multiple ice cores which is related to seasonal differences in ice density. Fourteau et al. (2017) showed that these variations can also be observed in ice during the last glacial period. These seasonal layers seal off bubbles at different depths, thus preserving air alternating between older and younger ages. Given a period of rapidly changing [CH_4], slow firn densification rates, and strong layering, the magnitude of the annual signal was found to be up to 40 ppb. Although the 40 ppb trapping signal is of similar magnitude as the estimated impact of excess CH_4 that we measured, it would not produce a continuing increase of [CH_4] over multiple melt-extraction cycles.

4.5. In Situ production of CH_4

The interiors of polar ice sheets are harsh environments for life due to the extreme cold, the limited liquid water, and the scarcity of nutrients. However, two micro-environments within ice sheets which may be suitable for life have been proposed; at triple-junctions between ice grains and on the

surface of dust particles, such as clays, where pressure or ion concentration prevents water from freezing and nutrients may be concentrated (Price, 2000; Tung et al., 2005; Price, 2007). In situ production fits many of our observations about excess CH_4, but only if the produced CH_4 would be adsorbed or trapped at the production site, e.g. onto particles.

In situ production of CH_4 would cause increased [CH_4] with depth (time) until either nutrients are exhausted or conditions (pressure, temperature) no longer support production. Time-dependent production would be observed as changes in the ratio of n^*_{xs} compared to the number of moles of Ca^{2+}. However, this relationship is remarkably consistent across the ∼30 ka time period covered by our GISP2 samples. This would imply that in the GISP2 ice core the production of CH_4 has ceased to occur at a significant rate in ice that is of at least 42,000 years old, the age of our youngest sample (2300 m). Measurement of shallower (younger) samples will be required to conclude whether in situ production exists in younger ice.

Microbial methane production is generally inhibited by the presence of oxygen. The partial pressure of oxygen in bubbles in the ice sheet is elevated above ambient levels due to the weight of overlying ice. The high oxygen pressures would likely prevent in situ microbial production. As was the case with the hypotheses of post-coring microbial production or in vitro production, if in situ microbial production of CH_4 did occur, it would be expected to have an isotopic composition lower than the estimated $\delta D(CH_4)_{xs}$ (Sect. 3.3). However, isotopic characterization experiments are typically conducted at much different temperature, pressure, and $\delta D(H_2O)$ conditions than would occur in an ice sheet. It is also possible that CH_4 is produced in situ by some abiotic process, however these mechanisms appear to require a high concentration of organic precursor (Jugold et al., 2012; Wang et al., 2017).

4.6. A deposition source of excess CH_4

Instead of being produced in the ice sheet, excess CH_4 may instead be carried from a CH_4 source to the ice sheet by some agent capable of absorbing hydrocarbons like clay minerals in dust, black carbon (BC), or organic carbon all of which are known to be abundant in the Greenlandic ice cores (Biscaye et al., 1997; Svensson et al., 2000).

Dust and clay minerals in the GISP2 and GRIP ice cores are well documented (Mayewski et al., 1997; Rasmussen et al., 2014; Schüpbach et al., 2018). Provenance of the dust is primarily from the Takla Makan desert in West China (Biscaye et al., 1997; Svensson et al., 2000; Bory et al., 2003).

In parts of this region, CH_4 diffuses through the soil from underlying fossil fuel reservoirs (Etiope and Klusman, 2002; Etiope et al., 2008) providing a viable source for CH_4 adsorption. While estimates of the adsorptive capacity of clay for abundances found in the GISP2 ice samples (calculated following Ji et al. 2012) show that this is a feasible mechanism, it is only feasible under ideal conditions for adsorption, retention of CH_4 during transport, and with efficient desorption during sample extraction (Appendix D, S. Table D.1). Many factors could limit the adsorptive capacity of clays such as the partial pressure of CH_4, the temperature of the clays, and the presence of water or other species during adsorption. Once in the atmosphere (transport time of days) and while still in contact with the atmosphere in the firn (centuries) the dust is in a much lower CH_4 environment and CH_4 would likely be released from the dust. Further, our estimates of the isotopic signature of excess CH_4 ($\delta D(CH_4)_{xs}$= -293‰) (Sect. 3.3) do not support this mechanism because our estimate is significantly more negative than typical emissions from seeps ($\delta D(CH_4)$ values of ∼-185 to -200‰, Quay et al. 1999; Etiope et al. 2007; Fischer et al. 2008).

A pyrogenic source, such as wildfires (-195 to -255‰, Quay et al. 1999; Snover et al. 2000), can not be definitively excluded by our estimates of $\delta D(CH_4)_{xs}$. In this case, CH_4 is more likely to be adsorbed and transported to the ice sheet by BC or organic matter. However, measurements of BC and organic matter are currently not available from a Greenlandic ice core. Identifying a source for excess CH_4 would benefit from estimate of $\delta^{13}C(CH_4)_{xs}$, but no record currently exists of $\delta^{13}C(CH_4)$ during DO-events from a Greenlandic ice core.

5. Considerations for atmospheric reconstructions

Rapid changes of $[CH_4]$ during the last glacial period, specifically those corresponding with D-O events, have been used extensively in the development of age scales for ice cores (Blunier et al., 1998; Brook et al., 2000; Kindler et al., 2014; Buizert et al., 2015). At the onset of D-O events, $[CH_4]$ increased by 60-220 ppb (Baumgartner et al., 2014), a large value in comparison to the impact of excess CH_4 on the ice core record (less than 40 ppb) implying that excess CH_4 probably has not affected $[CH_4]$-based age scales. One possible exception is DO-2, for which $[CH_4]$ only changed by 20-35 ppb (Baumgartner et al., 2012, 2014; Schilt et al., 2010). This event is important for gas-based chronologies because of the lack of other significant

variations around this time period. Ice core records of [CH_4] have also been used to reconstruct past radiative forcing with regards to the inferred climate changes of D-O cycles (Petit et al., 1999). The relatively small impact of excess CH_4 on the ice core [CH_4] record would not significantly alter these interpretations.

The geographic distribution of CH_4 sources in the past has been reconstructed from the difference in concentration between records of [CH_4] from Greenlandic and Antarctic ice cores (referred to as the "Inter-Polar Difference", or IPD, Chappellaz et al., 1997; Dällenbach et al., 2000; Brook et al., 2000; Mitchell et al., 2013; Baumgartner et al., 2012; Beck et al., 2018). During the last glacial cycle, the IPD ranged from ∼10-50 ppb with the Northern Hemisphere always having greater [CH_4] (Baumgartner et al., 2014). Excess CH_4, which is only observed in Greenlandic ice core samples, has likely caused the IPD to be overestimated during dusty time periods in Greenland. Since the impact of excess CH_4 on the Greenlandic records is of the same magnitude as the IPD, it will be critical to account for this effect.

Excess CH_4 also appears to have a large influence on the measured isotopic composition of CH_4 (Sect. 2.3). As discussed in Sect 3.3, assuming an isotopic signature ($\delta D(CH_4)_{xs}$=-293‰) similar to natural sources, the excess CH_4 contribution can account for much of the observed variability in the NGRIP $\delta D(CH_4)$ record (Bock et al., 2010b). Accordingly, some of the $\delta D(CH_4)$ variability in Bock et al. (2010b) is likely due to excess CH_4 and the conclusions of Bock et al. (2010b) should be confirmed using an Antarctic ice core. Although, a record of $\delta^{13}C(CH_4)$ has yet to be measured from a Greenlandic ice core during a period with dusty ice, $\delta^{13}C(CH_4)$ will likely also be affected by excess CH_4. Assuming an isotopic signature for excess CH_4 of $\delta^{13}C(CH_4)_{xs}$ equal to microbially produced CH_4 (∼-60 ‰, Quay et al. 1999; Bock et al. 2017), the impact of excess CH_4 may be up to ∼1.5‰. This magnitude of impact is significant when compared to centennial to millennial-scale variations as recorded in the Antarctic Vostok and EDML ice cores (Möller et al., 2013).

Recently, centennial-scale variability in [CH_4] during the last glacial period was identified in the WAIS Divide and Fletcher Promontory ice cores from Antarctica (Rhodes et al., 2017). These records confirmed the variability previously measured in the NEEM ice core (Chappellaz et al., 2013). The peak-to-peak magnitude of this variation was cited to be 8-12 ppb in the ice core record which was estimated to represent 8-24 ppb variations in the atmosphere (Rhodes et al., 2017). This is smaller than the impact of

excess CH_4 observed in Greenlandic ice cores meaning that centennial-scale variations could be confused for or masked by excess CH_4. We stress that we do not question the existence of the centennial-scale atmospheric variations for two reasons. First, excess CH_4 was absent in the discrete WAIS Divide samples (equivalent to contamination of -2 ppb $\pm$2 ppb, n=82), which closely replicated all modes of variability in the continuous [CH_4] measurements discussed in Rhodes et al. (2017). Second, the corrected GISP2 and NEEM discrete records also reproduce the centennial-scale variability in [CH_4] observed in the WAIS Divide record during DO-12 (Fig. 6, Sect. 3.2). The robust centennial-scale variations in both Greenlandic and Antarctic ice cores are important for the future development of high-precision gas age chronologies (Mitchell et al., 2013; Lee et al., 2018) and for understanding the climatic links to these variations of the CH_4 cycle in the past.

6. Implications for extremophiles

While no direct evidence of active microbes capable of producing greenhouse gases in "normal" ice has been reported, elevated concentrations have been observed for some biogenically produced gases such as CO_2, N_2O, and CH_4 (Sowers, 2001; Flückiger et al., 2004; Campen et al., 2003; Rhodes et al., 2013). Furthermore, several lines of circumstantial evidence support in situ CH_4 production, including the general association of high cell counts with high concentrations of dust (Abyzov et al., 1998; Tung et al., 2005; Rohde et al., 2008; Miteva et al., 2009, 2016). Viable cells in the GISP2 ice core have been estimated to account for 2.5-15% of the total cells present (Miteva et al., 2009, 2015), although methanogens have not been identified in normal ice samples (Tung et al., 2005; Rohde et al., 2008). One sample with an extremely high concentration of cells, 2238 m depth in the GISP2 ice core (Tung et al., 2005), was coincidentally among discrete [CH_4] samples inferred to be affected by excess CH_4 (Sect. 2.1).

The possibility of in situ CH_4 production could be tested with dust rich samples of younger ages (shallower depths), because the quantity of excess CH_4 should increase with age (Sect. 4.5). However, in GISP2 samples ranging from 42-75 ka we observed a consistent relationship between excess CH_4 and Ca^{2+} implying that CH_4 is not produced in situ at these depths (Sect. 3.4 and 4.5). If we assume no in situ production is observed because of nutrient limitation and that 95-99% of the limiting precursor for methanogenesis

was consumed by the age of our youngest sample, the representative e-folding time for the reaction is at most 9,000-14,000 years.

Production of biogenic gases in ice cores has been previously estimated by Price and Sowers (2004), Tung et al. (2005), and Rohde et al. (2008). Their estimates were based upon the idea that microbes in the ice sheet are only active enough to sustain themselves but not to reproduce. This implies that CH_4 is produced continuously in the ice core at constant rate. Following their calculation and using their empirically derived production rates for ice at -28° C ($\sim$5x10$^-$8 (g C-CH_4/g C-biomass)$\cdot$yr^{-1}), the estimated carbon mass of methanogens (19 femtograms C/cell, Price and Sowers 2004; Tung et al. 2005), the estimated percent of cells which are methanogens in normal ice (1/300, Price and Sowers 2004; Tung et al. 2005), the cell count at 2238 m depth ($\sim 10^5$ cells/mL, Tung et al. 2005), and the estimated percent of cells which are healthy (Miteva et al., 2009) yields an expected production of $\sim$0.00005 picomoles CH_4/g ice since 35,000 years. This estimate is much smaller than the estimates of n^*_{xs} of up to $\sim$0.01 picomoles CH_4/g ice in Sect. 3.2. Additionally, their assumption of continuous production is inconsistent with the observed constant ratio of n^*_{xs} and Ca^{2+} in the GISP2 ice core (Sect. 3.2). If the excess CH_4 we observe is due to metabolism within the ice sheet, then microbial metabolism in normal ice is more vigorous than required for simply sustaining life.

7. Conclusions

We discuss a new process able to distort the atmospheric record preserved in ice cores by elevating the measured concentration of CH_4. This process is related to a commonly used measurement technique, where the sample is melted for prolonged periods (15-30 minutes) to liberate air from within the sample. The elevated values were observed for "normal" ice core samples (ice core samples which are not affected by melt layers or entrained sediment) and differs from other non-atmospheric processes such as the very brief spikes resulting from in situ processes observed by (Rhodes et al., 2013) and from annual-layer trapping signals (Rhodes et al., 2013, 2016), which are localized reversals of the depth-age relationship. This additional CH_4, referred to as "excess CH_4", was only observed in samples with high concentrations of dust and impurities and not observed in Antarctic ice core samples and Greenlandic ice core samples with low dust concentrations. Several potential sources of CH_4 are proposed, although none perfectly match our observations.

The possible mechanisms which we consider the most likely explanations for the excess CH_4 include the transport of CH_4 adsorbed onto dust or BC particles from remote regions and in situ production of CH_4 on or in dust particles. However, our observations cannot exclude the mechanism of abiotic in vitro production (i.e. CH_4 produced during the melt-extraction step of sample analysis). Both of our preferred pathways focus on the adsorption of CH_4 onto the particle and subsequent desorption of CH_4 during the melt-extraction step of sample analysis when liquid water is present. Since in situ methanogenesis would gradually increase the abundance of CH_4 in the ice sheet, measurement of younger ice could provide valuable information to distinguish between the two proposed mechanisms.

As future ice core records of CH_4 gain precision and resolution, a more direct approach to measuring or negating the effects of excess CH_4 will need to be developed. One possible way forward could be to measure a suite of samples with a "dry" extraction technique where air is extracted by mechanically crushing the ice or through sublimation (Etheridge et al., 1996, 1998; Sapart et al., 2011; Schmitt et al., 2011), which may not be affected by excess CH_4 in the same way because the sample is not melted. Comparing to $[CH_4]$ records measured with a melt-extraction technique ("wet" extraction) could both test our proposed ideas about the desorption of CH_4 in the presence of liquid water and provide a reference for Northern Hemisphere CH_4 concentrations during dusty intervals. No evidence of excess CH_4 was observed in records measured with continuous flow analysis, potentially due to the short time period before the gas is separated from the liquid stream. Therefore, an independently calibrated continuous $[CH_4]$ record from a Greenlandic ice core may also provide a reference, although currently no such record is available.

While it is clear that excess CH_4 will need to be accounted for when interpreting records of $[CH_4]$ and the stable isotopes of CH_4, the presence of excess CH_4 may be evidence of microbial activity occurring within the Greenland ice sheet. The abundance of cells has been observed to vary in ice cores with the concentration of dust (Abyzov et al., 1998; Tung et al., 2005; Miteva et al., 2016), implying that an empirical relationship also with excess CH_4. Methanogenesis in such a harsh environment tests the limits of life, possibly providing an analogue for early life on Earth or possible life on other planets.

Acknowledgements

This work was funded by grants from the US National Science Foundation PIRE award 0968391. Research performed at the University of Bern has received funding from the European Research Council (ERC) under the European Union s Seventh Framework Programme FP7/2007-2013 ERC grant 226172 (ERC Advanced Grant Modern Approaches to Temperature Reconstructions in Polar Ice Cores (MATRICs)) and the Swiss National Science Foundation. We thank Jonas Beck and Barbara Seth for discussion and their expertise in the measurement of the stable isotope composition of CH_4.

Data Availability

Datasets related to this article can be found at: `https://www.ncdc.noaa.gov/paleo/study/27610`.

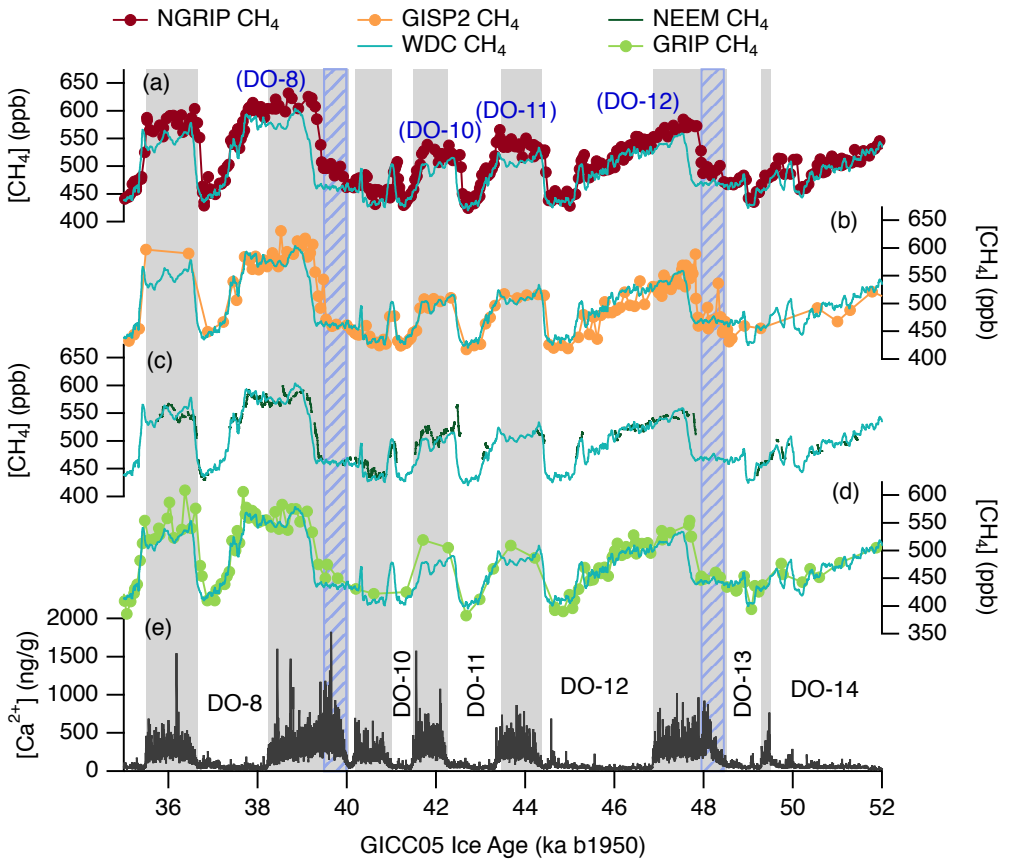

Figure 1: Comparison of $[CH_4]$ histories from Greenlandic ice cores: (a) NGRIP (Baumgartner et al., 2014), (b) GISP2 (Brook et al. 1996, 2000 and previously unpublished measurements will be made available at NOAA National Centers for Environmental Information (Link), (c) NEEM continuous (Chappellaz et al., 2013), and (d) GRIP (Blunier and Brook, 2001; Flückiger et al., 2004; Landais et al., 2004) to the WAIS continuous record (Rhodes et al., 2015), and to (e) Ca^{2+} concentrations (Rasmussen et al., 2014; Schüpbach et al., 2018). All $[CH_4]$ records have been translated onto the NGRIP ice age scale. DO-events as expressed by $[CH_4]$ are labeled in blue with parentheses, and as expressed in Ca^{2+} are labeled in black. Gray bars highlight periods of high Ca^{2+} concentrations. Hatched boxes indicate intervals where discrete records diverge from the WAIS Divide and NEEM continuous records.

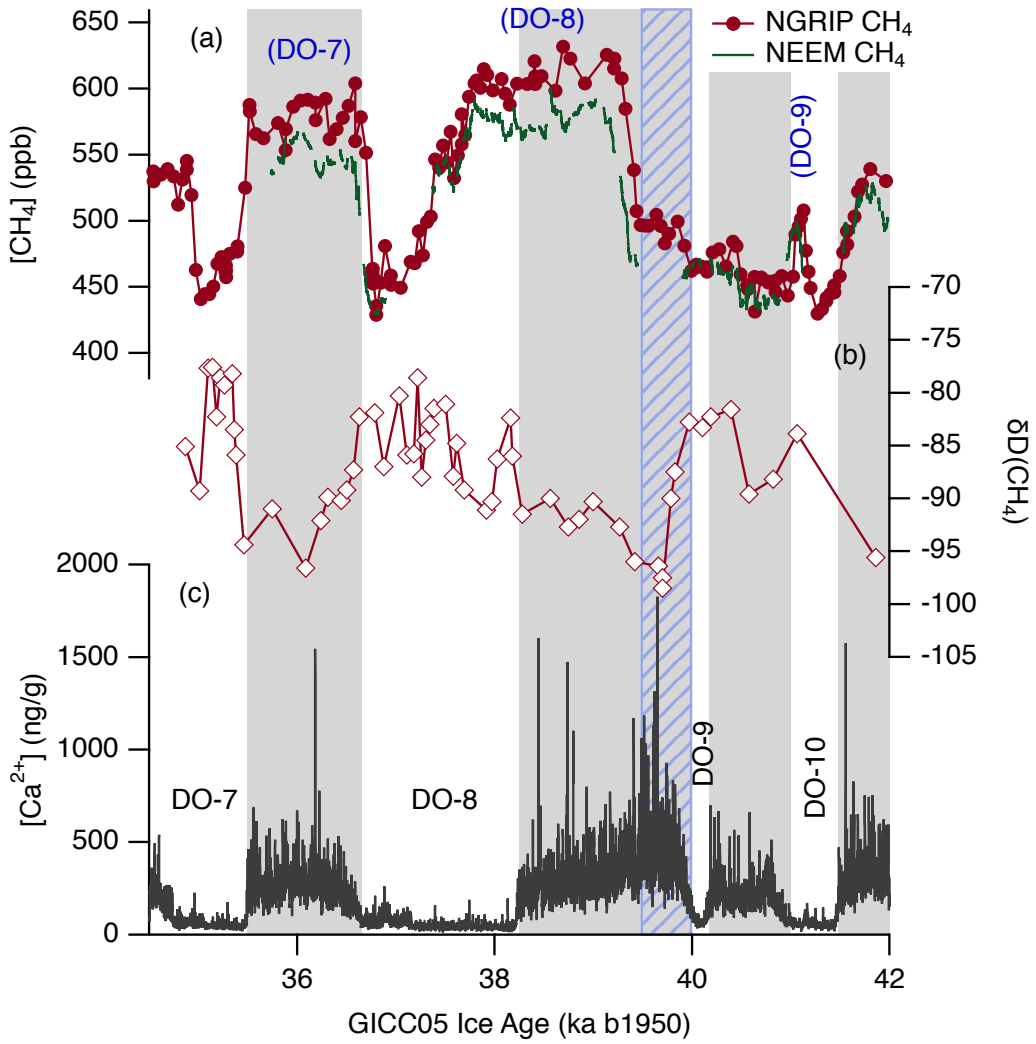

Figure 2: Records of (a) NGRIP $[CH_4]$ (Baumgartner et al., 2014), (b) $\delta D(CH_4)$ from NGRIP (Bock et al., 2010b) plotted on the NGRIP GICC05 ice age scale, and (c) NGRIP Ca^{2+} (Rasmussen et al., 2014; Schüpbach et al., 2018). $[CH_4]$ records from the NEEM (Chappellaz et al., 2013) and NGRIP ice cores show inconsistencies between records. Excursions observed in the stable isotope record of CH_4 from the NGRIP ice core occur at similar depths as the discrepancies in $[CH_4]$ and in ice with high concentrations of Ca^{2+}. DO-events as expressed by $[CH_4]$ are labeled in blue, and as expressed by Ca^{2+} are labeled in black.

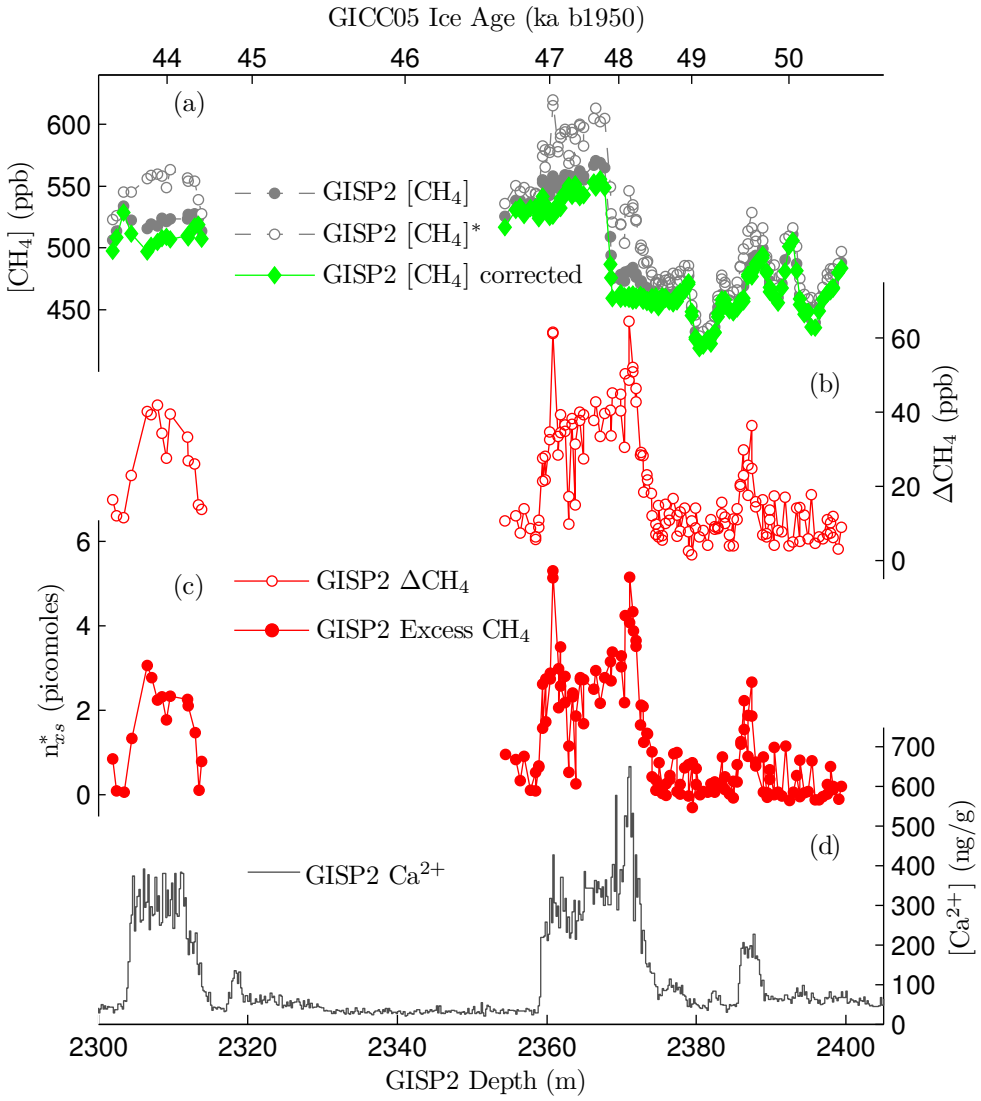

Figure 3: (a) $[CH_4]$ (b) ΔCH_4 and (c) excess CH_4 from the GISP2 ice core are plotted against depth. (a) includes the first set of GC measurements from each sample ($[CH_4]$, gray circles), the second set ($[CH_4]^*$, open gray circles), and a "corrected" value (green diamonds). (d) Calcium concentrations from the GISP2 are plotted for comparison (Mayewski et al., 1997).

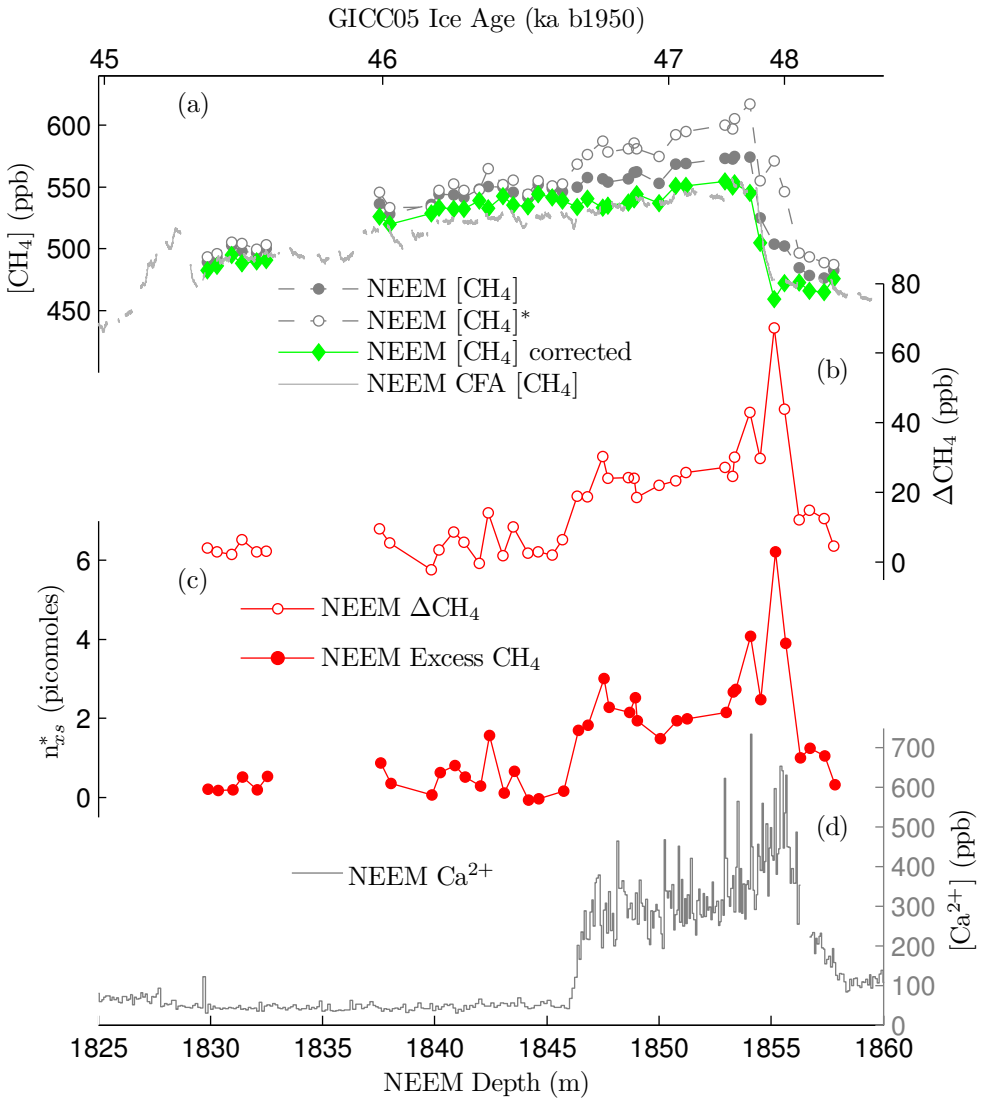

Figure 4: CH_4 results from the NEEM ice core are plotted against depth, same as Fig. 3. The NEEM Ca^{2+} record is sub-sampled from an ultra-high resolution CFA dataset (Schüpbach et al., 2018).

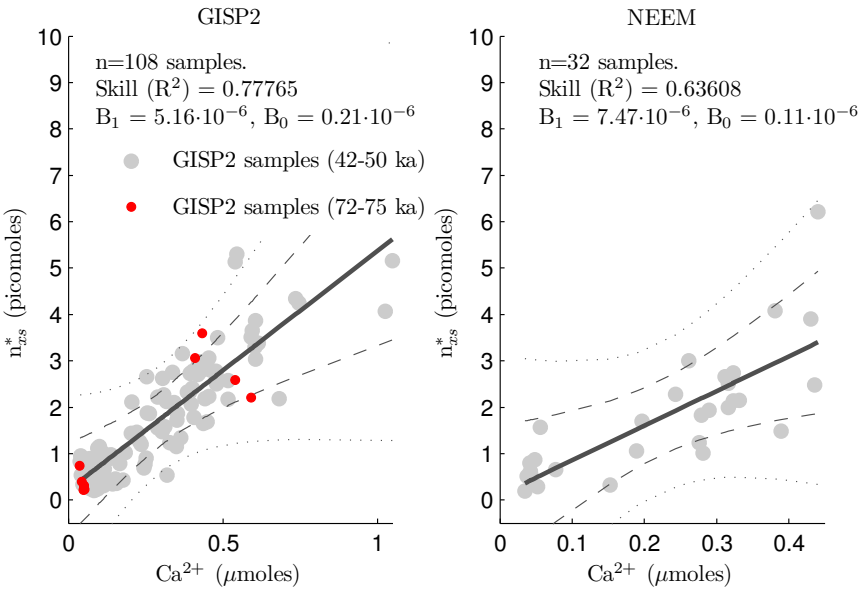

Figure 5: Regression of n^*_{xs} against the quantity of calcium in GISP2 and NEEM samples (Mayewski et al., 1997; Schüpbach et al., 2018) following methods of York et al. (2004). For GISP2 samples with an age between 42 and 50 ka (gray dots), the skill of the regression is R^2=0.78 with 5.2 $\pm$ 0.5 μmoles (95% CI) of excess CH_4 per mole of calcium, and R^2=0.64 with 7.5 $\pm$ 2.0 μmoles of excess CH_4 per mole of calcium for NEEM samples. Older GISP2 samples, dating between 72-75 ka, are plotted as red dots.

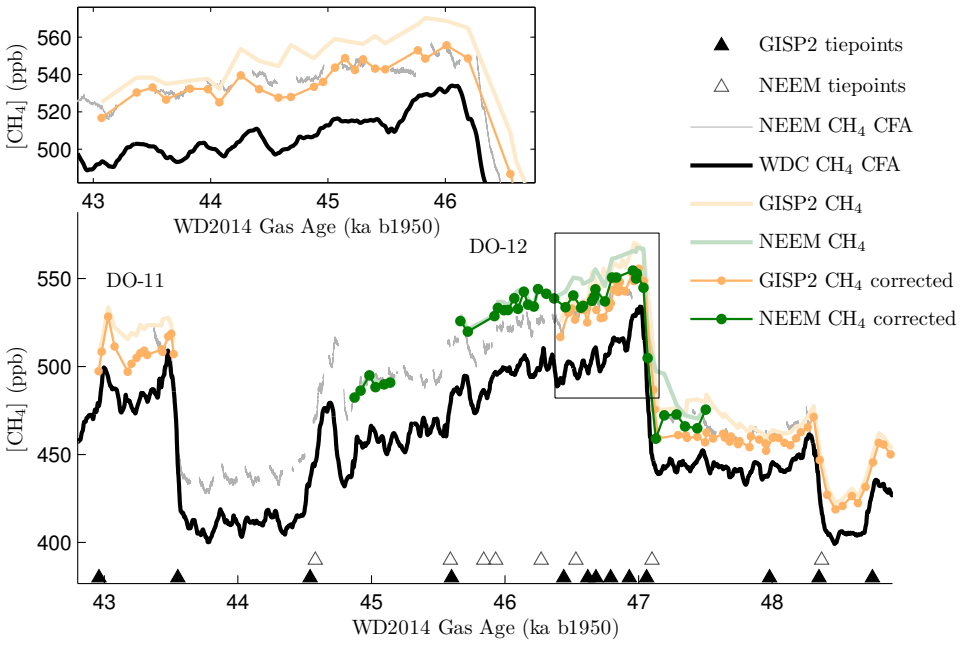

Figure 6: Measured [CH_4] and concentrations after an ad hoc correction for excess CH_4 from the GISP2 (orange) and NEEM (Green) ice cores. Discrete measurements are compared to the WAIS Divide and NEEM continuous records (black and gray, respectively). Both the GISP2 and NEEM data were synchronized to the WD2014 age scale (Buizert et al., 2015).

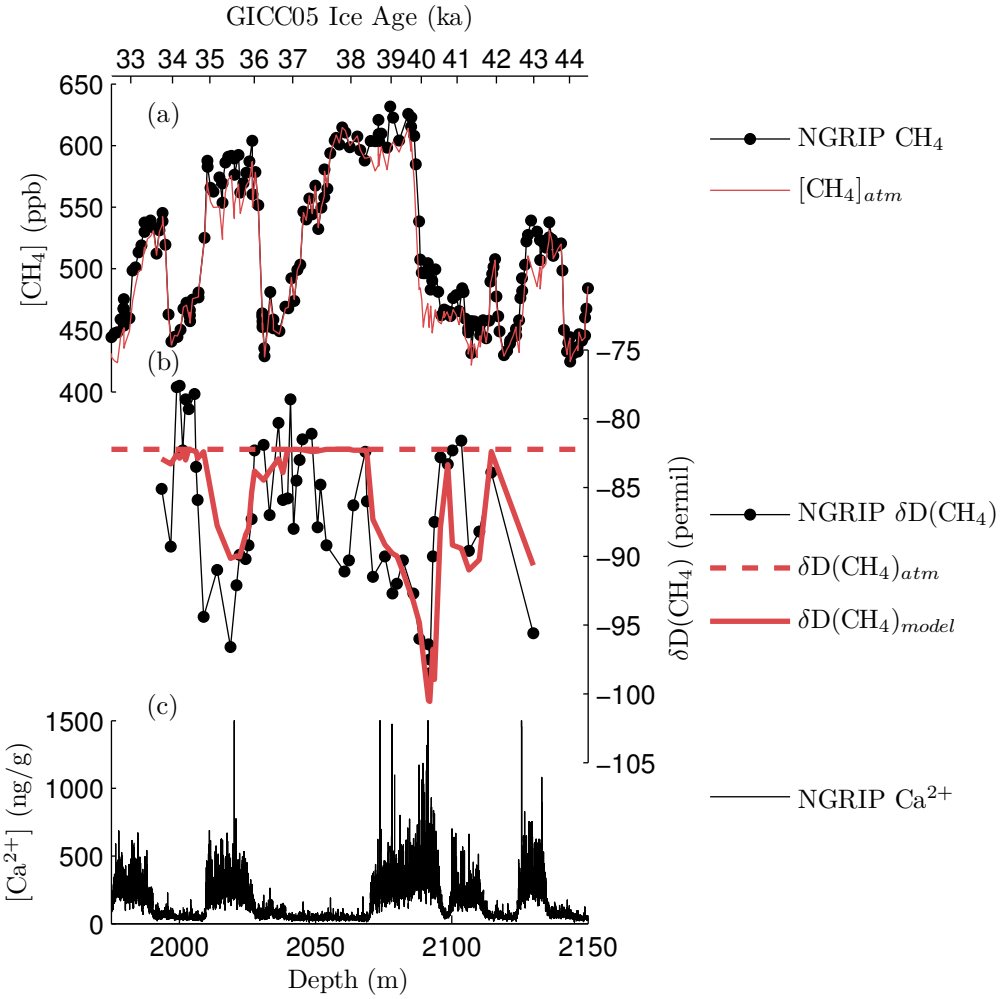

Figure 7: A modeled ice core history of δD(CH_4) with a two-component mixing model with end-members of atmospheric air and excess CH_4. Black lines and circles are measurements of (a) [CH_4] (Baumgartner et al., 2014), (b) δD(CH_4) (Bock et al., 2010b), and (c) [Ca^{2+}] (Rasmussen et al., 2014) from the NGRIP ice core. Red line in panel (a) is the atmospheric component in the model. Panel (b) also shows model results for $\delta D(CH_4)_{atm}$ (dashed) and $\delta D(CH_4)_{model}$ (solid) based on an empirical relationship between enrichments of [CH_4] and concentrations of Ca^{2+}.

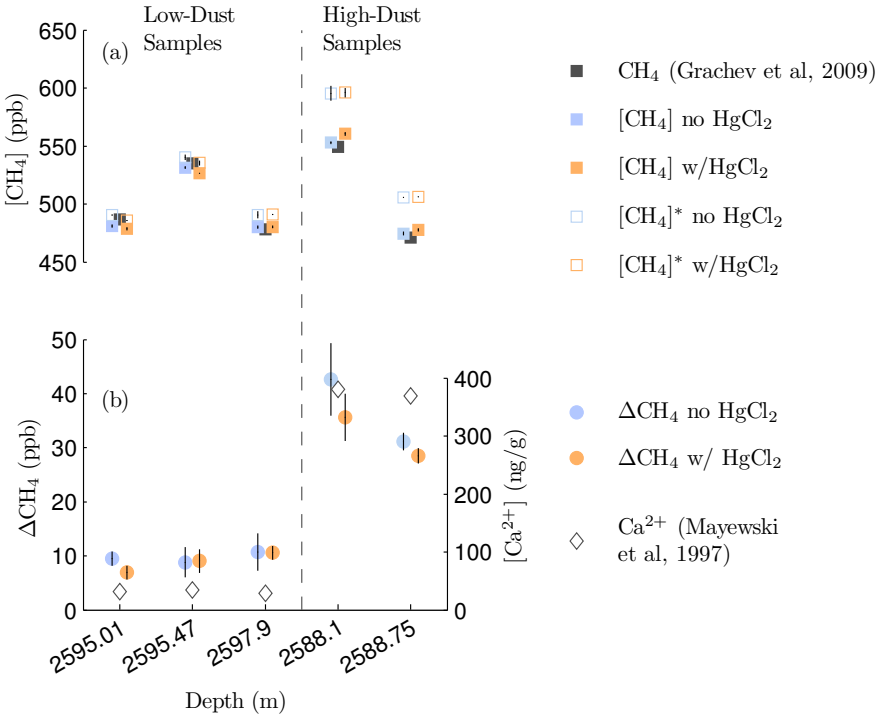

Figure 8: Inhibition experiments. Five GISP2 sample depths were measured in replicate; two dust-rich sample depths and three low-dust samples. One replicate of each sample depth was poisoned with $HgCl_2$ (orange) while the other was used as a control (blue). (a) Filled squares are measurements after the first extraction ($[CH_4]$), open squares are measurements after the second extraction ($[CH_4]^*$). $[CH_4]$ values match previous measurements of $[CH_4]$ from Grachev et al. (2009) (gray squares). (b) The difference between the first and second set of measurements (ΔCH_4) (circles) show a good correspondence with the dust concentration at those sample depths (open diamonds).

Table 1: Coefficient of determination (R^2) of release/production or n^*_{xs} in dust-rich GISP2 and NEEM samples compared to moles of chemical species in the ice sample (Mayewski et al., 1997; Schüpbach et al., 2018). Interpolated GISP2 ion concentrations are a weighted mean of the 20 cm binned average values. NEEM ion concentrations and dust counts are sub-sampled for the depth range of our NEEM samples (Schüpbach et al., 2018). Statistical p-values for correlation are all <0.0001.

	n	Na^+	NH_4^+	K^+	Mg^{2+}	Ca^{2+}	Cl^-	NO_3^-	SO_4^{2-}	Dust #
T_{melt}=26° C										
GISP2	42	0.67	0.20	0.66	0.75	0.78	0.58	0.33	0.67	
NEEM	27					0.64				0.59
T_{melt}=0° C										
GISP2	42	0.25	0.06	0.28	0.34	0.37	0.16	0.12	0.25	
NEEM	27					0.54				0.49

Appendix A. CH_4 records on gas-age scales

Appendix B. Calculation of CH_4 partitioning constant

During our gas extraction process some air is dissolved into the melt water and is not expelled during the refreeze step, unlike in systems which flush the melt water with a carrier gas or slowly refreeze the melt water. Since CH_4 is more soluble than nitrogen or oxygen, the major species in air, the measured CH_4 concentration ($[CH_4]$) is lower than when the air was trapped in the ice core. Dissolution of gases into the melt water is a kinetic process and due to the short melt-refreeze cycle (approximately 30 minutes) the uptake of gases into the melt water is likely halted before thermodynamic equilibrium is reached. This means the dissolved CH_4 is likely lower than the capacity of the melt water (undersaturated) and an empirical correction is needed to accurately estimate the quantity of CH_4 trapped in the refrozen sample. Previous studies estimated that dissolved CH_4 accounts for $\sim$1.7% of the total CH_4 from an ice core sample for the OSU system (Grachev et al., 2009; Mitchell et al., 2013). Although this estimate was calculated in a different way, it agrees well with estimates made here.

The effects of differential solubility will cause $[CH_4]$ in the headspace to increase after the second melt-refreeze. The mean $[CH_4]$ value of the second measurement set ($[CH_4]^*_{gas}$) minus the mean value of the first measurement set ($[CH_4]_{gas}$ is referred to as ΔCH_4.

$$\Delta CH_4 = [CH_4]^*_{gas} - [CH_4]_{gas} \tag{B.1}$$

Positive ΔCH_4 values are observed in the vast majority of our samples (Fig. 3 and 4) including BFI samples and samples assumed to be unaffected by excess CH_4. An increase in concentration is caused by the decrease in sample pressure in the flask as sample air is consumed during the first sequence of GC measurements (consuming $\sim$60% of the sample air). The reduction in pressure causes CH_4 to degas during the second melt-refreeze cycle resulting in higher $[CH_4]$ values for the second set of measurements compared to the first set of measurements. In these samples, ΔCH_4 is related to the total air content (TAC), $[CH_4]$, the size of the sample, the relative solubility of CH_4 compared to major air components, and the relative diffusion rates and extent of progress toward solubility equilibrium of CH_4 in comparison to N_2 and O_2 during the first melt-extraction and expulsion of gases during the subsequent refreeze.

To estimate the amount of CH_4 left in the solution/ice after the first refreeze, we define and empirically estimate the "partitioning constant", $K_{partition}$. $K_{partition}$ is the partial pressure of CH_4 in the headspace divided by the concentration of the CH_4 trapped in the ice following the first extraction (units of MPa·(mol/kg)$^{-1}$ and is calculated for each sample. This parameter is similar to Henry's constant, which describes the partial pressure of gas over the dissolved species in water under the conditions of thermodynamic equilibrium. In this definition, and in the absence of release/production of CH_4 during analysis, Henry's constant places a lower limit on the value of $K_{partition}$ because in the first extraction CH_4 is being absorbed into melt water.

The second melt-refreeze cycle begins closer to equilibrium and we assume that the flux of CH_4 out of solution during this step brings [CH_4] near equilibrium. If equilibrium is not reached during the second melt-refreeze, then our calculation will underestimate n^*_{xs} (Appendix C). Given this assumption, the total number of moles of CH_4 in the flask, both the dissolved and gas phase, can be estimated and $K_{partition}$ can be calculated by the following system of equations:

$$n_{total} = n_{ice\,core} = n_{gas} + n_{aq} \tag{B.2}$$

$$n^*_{total} = n^*_{gas} + n^*_{aq} = f \cdot n_{gas} + n_{aq} \tag{B.3}$$

$$n_{gas} = [CH_4]_{gas} \cdot \frac{m \cdot TAC \cdot P_{STP}}{R \cdot T_{STP}} \tag{B.4}$$

$$n^*_{gas} = [CH_4]_{gas} \cdot \frac{m \cdot TAC^* \cdot P_{STP}}{R \cdot T_{STP}} \tag{B.5}$$

$$[CH_4]_{aq} = \frac{n_{aq}}{m} \tag{B.6}$$

$$K_{partition} = \frac{p}{[CH_4]_{aq}} \tag{B.7}$$

$$H = \frac{p^*}{[CH_4]^*_{aq}} \tag{B.8}$$

$$n^*_{aq} = [CH_4]^*_{aq} \cdot m = m \cdot \frac{p^*_{CH4}}{H} \tag{B.9}$$

Variables demarcated with "*" indicate they are associated with the second melt-refreeze cycle and second set of measurements. The sample mass is given as "m" in units of grams. "R" is the ideal gas constant (8.314

$J \cdot mol^{-1} \cdot K^{-1}$). TAC is in units of cc air (STP)/gram ice and is a byproduct of [CH_4] measurements. "n" is the number of moles of CH_4 with the phase or origin identified by the subscript. "p" is the partial pressure of CH_4 in the headspace while the sample is melted (Pa). In eqn. B.4 and B.5, "n_{gas}" and "n^*_{gas}" are the number of moles of CH_4 in the gas phase after the first and second melt-refreeze extraction and are calculated from the TAC and the measured [CH_4] of the sample. In eqn. B.8 and B.9, "H" is the Henry's Law solubility constant of CH_4 (for water at 0° C, H=43.3 $MPa \cdot (mol/kg)^{-1}$; at 26° C, H=73.3 $MPa \cdot (mol/kg)^{-1}$) (Lide, 2004). The variable f is the fraction of air remaining in the headspace after the first set of measurements is complete and is calculated from the pressure of the last measurement of the set and an estimate of volume of the flask.

p can not be directly measured but can be estimated by the ideal gas law which is dependent on the temperature of air within the flask as the sample is melted. This temperature is not well known and changes throughout the melt-refreeze process. We tested a range of temperatures from a lower limit of 0° C to an upper limit of 26° C, the measured temperature of a sample immediately after the 30 minute melt cycle. In the OSU system, under this temperature and pressure range CH_4 overwhelmingly exists as in the gas phase, rather than in the dissolved state, and assumptions about temperature have limited impact on our results.

Equations B.2-B.9 simplify to solve for $K_{partition}$:

$$K_{partition} = \frac{n_{gas}}{n^*_{gas} \cdot (1 + m \cdot R \cdot T_{melt} \cdot V^{-1}_{headspace} \cdot H^{-1}) - f \cdot n_{gas}} \cdot \frac{m \cdot R \cdot T_{melt}}{V_{headspace}} \tag{B.10}$$

Where T_{melt} is the temperature of gas during the melt-refreeze cycle (either 0° C or 26° C), and $V_{headspace}$ is the volume of the headspace in the flask. T_{melt}=26^o C, is based on measurements of the temperature of melt water following a third melt-extraction and is considered the maximum temperature a sample reaches before re-immersion into the cold-bath for refreezing.

$K_{partition}$ was calculated for each sample individually (S. Fig B.2). Since this is an empirical quantification, any process which could affect the aqueous-gas exchange of CH_4 during the extraction process (such as the ion activity, sample water temperature, or the expulsion of dissolved gases during freezing) is incorporated in this term.

In general, our determinations of $K_{partition}$ are higher than equilibrium (T=)^o C) (Lide, 2004) indicating that dissolution of CH_4 into the water was incomplete during the first extraction. However, enough CH_4 is dissolved that under the reduced pressure during the second gas extraction out-gassing of CH_4 occurs. The exceptions are GISP2 and NEEM samples with high concentrations of Ca^{2+}. In both of these cases, ΔCH_4 indicates that more CH_4 out-gassed from the melt water during the second melt-refreeze cycle than would be possible even if CH_4 dissolution had reached equilibrium during the first melt-extraction.

We categorize samples into groups based on their drill site as well as if $K_{partition}$ is less than equilibrium (H). A baseline $K_{partition}$ for each group ($\overline{K}_{partition}$, Table B.1), calculated as the mean of each grouping, describes the typical partitioning of CH_4 between dissolved and gas phases after the first extraction. $\overline{K}_{partition}$ can be used to estimate an expected ΔCH_4. The difference between the expected ΔCH_4 and the measured ΔCH_4 is an estimate of n^*_{xs} (Appendix C).

For low-dust GISP2 ice samples, those in which $K_{partition}$ is greater than H, the mean difference between measured ΔCH_4 and the expected value calculated from $\overline{K}_{partition}(T_{melt} = 0^o C)$ is 1.2 ppb $\pm$ 2.4 ppb, n=46 (Fig. B.3). The non-zero difference is because of the non-linear relationship between $K_{partition}$ and ΔCH_4. For WAIS Divide and bubble free ice samples, which we believe are unaffected by excess CH_4, difference between the measured and expected ΔCH_4 is 3.5 ppb $\pm$ 4.9 ppb (n=82) and -0.1 ppb $\pm$ 5.0 ppb (n=69), respectively. The uncertainty is similar to the combined uncertainty of the first and second set of measurements.

Table B.1: Calculated $\overline{K}_{partition}$ for different ice cores (MPa·(mol/kg)$^{-1}$). NIST value is the Henry's Constant for CH_4 (Lide, 2004).

Temp.	**NIST**	WAIS	SPICE	GISP2 low-dust	GISP2 high-dust	NEEM low-dust	NEEM high-dust	BFI
0° C	39.6	43.9	42.9	49.3	30.2	45.8	25.7	72.4
26° C	73.3	61.6	57.8	79.8	49.1	89.9	38.6	114.1

Appendix C. Calculation of excess CH_4

The mass balance equation describing the second melt-refreeze cycle (Eqn. B.3) can be rewritten to include the potential release/production of CH_4 (n^*_{xs}).

$$(f \cdot n_{gas} + n_{aq}) + n^*_{xs} = n^*_{gas} + n^*_{aq} \tag{C.1}$$

The first two terms on the left side of this equation describe the quantity of CH_4 remaining in the flask after the first set of measurements and before the second melt-refreeze step. The right side of the equation describes the quantity of CH_4 after the second melt-refreeze. The difference between the two sets of terms gives us the quantity of CH_4 released or produced during the second melt-refreeze step (n^*_{xs}).

The fraction of CH_4 trapped in the refrozen melt-water following the two melt-refreeze steps (n_{aq} and n^*_{aq}) is determined from the empirically derived $\overline{K}_{partition}$ and H, respectively.

$$n_{aq} = m \cdot \frac{p}{\overline{K}_{partition}} \tag{C.2}$$

$$n^*_{aq} = m \cdot \frac{p^*}{H} \tag{C.3}$$

As in Sect. Appendix B, 'm' represents the mass of the sample, 'p' is the partial pressure of CH_4 in the headspace during the melt-extraction, and H is the equilibrium solubility constant.

From this set of equations, n^*_{xs} can be solved following:

$$n^*_{xs} = n^*_{gas} \cdot (1 + \frac{m \cdot A}{H}) - n_{gas} \cdot (f + \frac{m \cdot A}{\overline{K}_{partition}}) \tag{C.4}$$

$$\tag{C.5}$$

Where A is the conversion factor between p and n_{gas} (A= $R \cdot T_{melt} \cdot V^{-1}_{headspace}$).

Two main assumptions have been made in order to calculate n^*_{xs}. First, the distribution between gas and dissolved phases of CH_4 reaches equilibrium during the second melt-refreeze. If CH_4 is not able to completely degas from solution and reach equilibrium during this step, than some aqueous CH_4 is

unaccounted for and our estimates of n^*_{xs} are too low. The second assumption is the temperature of the water during the melt-refreeze step which determines equilibrium solubility (H). As in the case of $\overline{K}_{partition}$, the calculation of n^*_{aq} was repeated assuming T_{melt}=0° C and 26° C. We also repeat the calculation of n^*_{xs} assuming no dissolution of CH_4 (H=0, a maximum estimate for n^*_{xs}) and repeat the calculation assuming that gases reach thermodynamic equilibrium during the first melt-refreeze ($K_{partition}$=H, a minimum estimate of n^*_{xs}). Typically, the difference between the maximum scenario and our estimate was small (0.33 picomoles given T_{melt}=26° C, and 0.83 picomoles given T_{melt}=0° C) and is larger at low quantities of n^*_{xs}. At low values of n^*_{xs} some of ΔCH_4 is attributed to out-gassing of CH_4, however in the maximum scenario ΔCH_4 is solely attributed to excess CH_4.

Appendix D. Calculation of adsorptive capacity

An estimate of the concentration of dust in the GISP2 ice core was given in Ram and Koenig (1997) and Ram et al. (2000). We use these data as a maximum estimate for the abundance of clay minerals in the GISP2 ice samples. Adsorption of CH_4 by clays depends on the mineralogy. Clay in the GISP2 and GRIP ice cores was characterized for several periods during the last glacial period and found to be dominated by illite (Biscaye et al., 1997; Svensson et al., 2000; Újvári et al., 2015). The abundance of illite relative to other clay minerals was relatively constant throughout the time period studied. Estimation of the adsorption capacity follow Ji et al. (2012), and use the amount of dust in the sample, the clay composition of the dust, and by assuming a partial pressure and temperature during adsorption (Table D.1).

Under ideal conditions, with high partial pressures of CH_4 during adsorption, the resulting adsorptive capacity of clays in the GISP2 ice core would be greater than the calculated n^*_{xs}. Such conditions may exist in soils with seepage of geologic CH_4. However, our calculated value of n^*_{xs} only accounts for excess CH_4 released/produced during the second melt extraction and not the total excess CH_4 that could be released/produced given additional time. Values given in Table D.1 are therefore a maximum value.

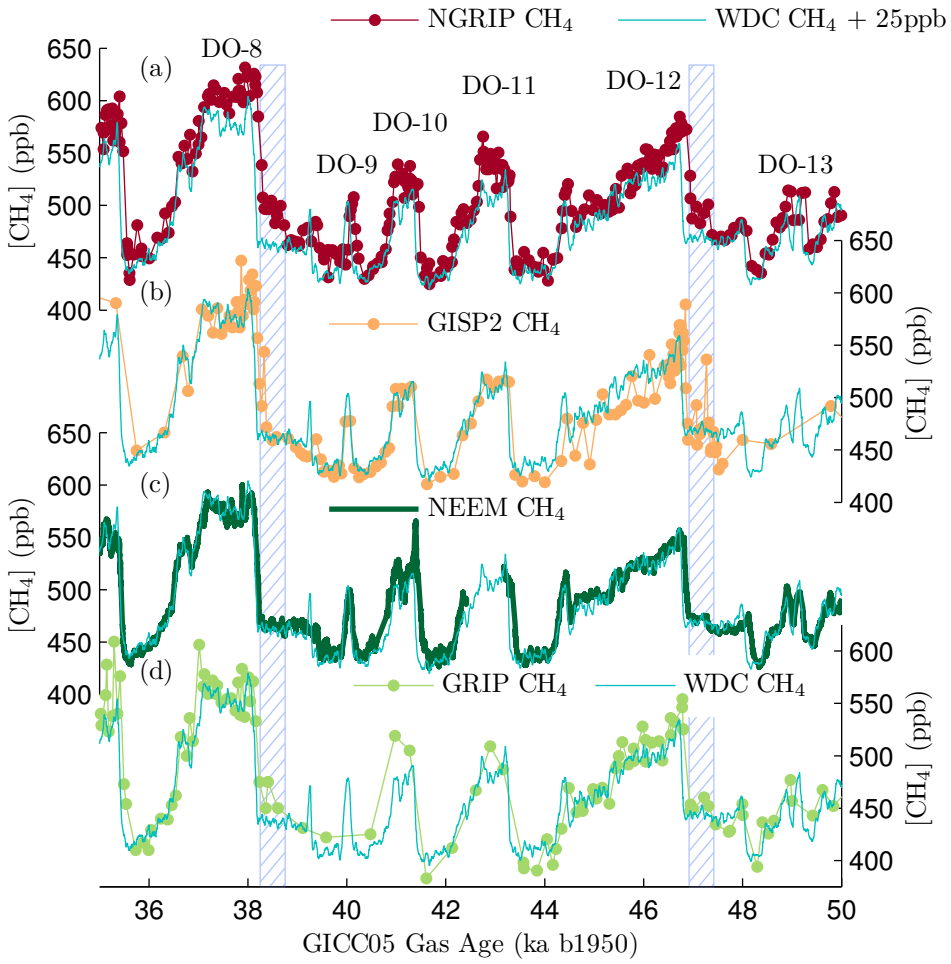

Figure A.1: Comparison of $[CH_4]$ histories from Greenlandic ice cores: (a) NGRIP (Baumgartner et al., 2014), (b) GISP2 (Brook et al. 1996, 2000 and previously unpublished measurements available at `https://www.ncdc.noaa.gov/paleo/study/27610`, (c) NEEM (Chappellaz et al., 2013), and (d) GRIP (Blunier and Brook, 2001; Flückiger et al., 2004; Landais et al., 2004) to the WAIS Divide continuous $[CH_4]$ record Rhodes et al. (2015). The WAIS Divide $[CH_4]$ values have been shifted to account for the interpolar concentration difference of $[CH_4]$. Greenland records are plotted on their respective GICC05 gas age scales (Rasmussen et al., 2013; Kindler et al., 2014; NEEM Community Members, 2013). The WD2014 gas age scale has been reduced by a constant 0.64% following (Buizert et al., 2015) to translate the WAIS Divide $[CH_4]$ record to the GICC05 age scale. Hatched boxes indicate intervals where discrete records diverge from continuous records.

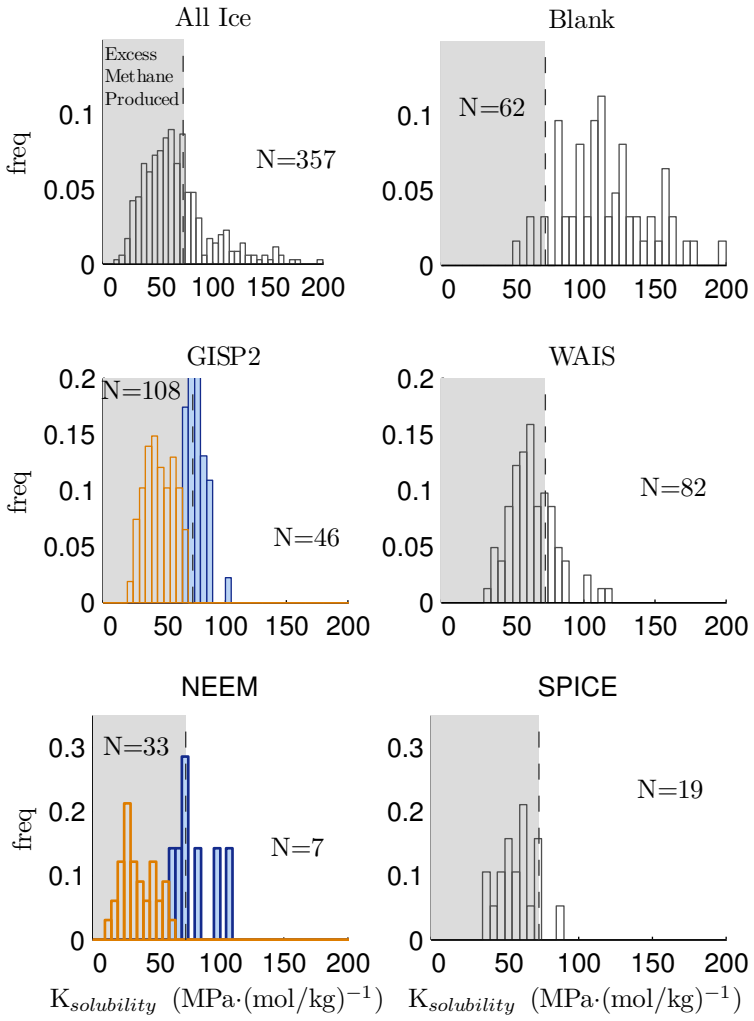

Figure B.2: Measured partitioning constant ($K_{partition}$) of different ice cores. For the GISP2 and NEEM ice cores, orange bars represent dust-rich ice samples where excess CH_4 was observed and blue bars represent low-dust samples where excess CH_4 was absent. Henry's constant for CH_4, (vertical dashed lines) was calculated assuming T=26° C (Lide, 2004). Values smaller than Henry's constant imply release or production of CH_4 during the extraction process.

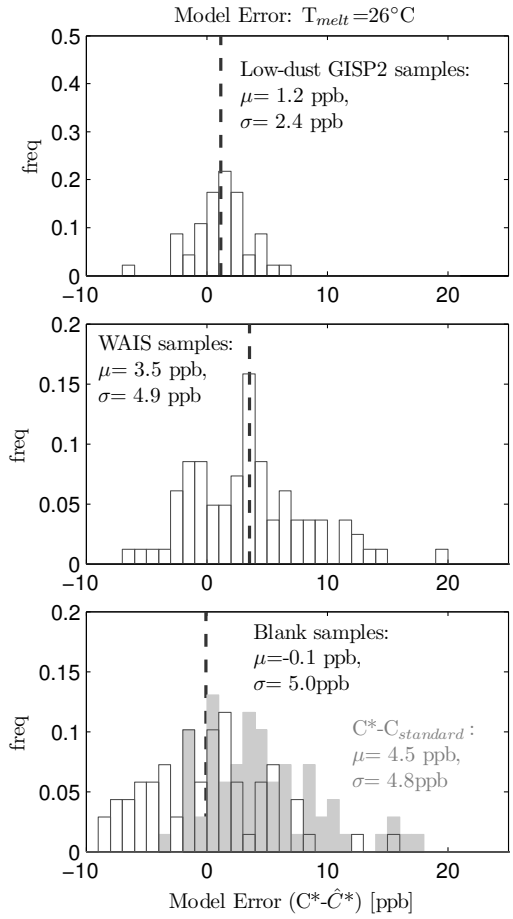

Figure B.3: Measured minus expected ΔCH_4 for different low-dust ice samples used as a baseline for $\overline{K}_{partition}$. These samples were assumed to have no excess CH_4 and set the empirical relationship for solubility.

Table D.1: Estimate of the adsorptive capacity of clays in the GISP2 ice core under different adsorptive scenarios for temperature and abundance of CH_4 following Ji et al. (2012). This estimate assumes that all dust in the ice core is composed of clays with a constant composition (Biscaye et al., 1997; Svensson et al., 2000) and abundance given by Ram and Koenig (1997) and Ram et al. (2000). Values are listed as the fraction of potential clay adsorptive capacity, i.e. the ratio of n^*_{xs} over the adsorptive capacity (n_{cap}). Values less than 1 indicate that an estimated adsorptive capacity greater than the observed release/production of n^*_{xs}. It is important to note that n^*_{xs} represents only the excess CH_4 released/produced during the ∼30 minute second melt-refreeze step of analysis .

$\frac{n^*_{xs}}{n_{cap}}$	T=0° C	T=30° C
P_{CH4}=1 atm	0.014	0.021
P_{CH4}=0.1 atm	0.137	0.215
P_{CH4}=0.01 atm	1.37	2.15

Abyzov S., Mitskevich I. and Poglazova M. (1998) Microflora of the deep glacier horizons of central Antarctica. *Microbiology (Moscow, Russ. Fed.)* **67**, 451–458.

Anklin M., Barnola J. M., Schwander J., Stauffer B. and Raynaud D. (1995) Process affecting the CO_2 concentrations measured in Greenland ice. *Tellus B* **47**, 461–470.

Aydin M., Montzka S. A., Battle M. O., Williams M. B., De Bruyn W. J., Butler J. H., Verhulst K. R., Tatum C., Gun B. K., Plotkin D. A., Hall B. D. and Saltzman E. S. (2010) Post-coring entrapment of modern air in some shallow ice cores collected near the firn-ice transition: evidence from CFC-12 measurements in Antarctic firn air and ice cores. *Atmos Chem Phys* **10**, 5135–5144.

Baumgartner M., Kindler P., Eicher O., Floch G., Schilt A., Schwander J., Spahni R., Capron E., Chappellaz J., Leuenberger M., Fischer H. and Stocker T. F. (2014) NGRIP CH_4 concentration from 120 to 10 kyr before present and its relation to a $\delta^{15}N$ temperature reconstruction from the same ice core. *Clim Past* **10**, 903–920.

Baumgartner M., Schilt A., Eicher O., Schmitt J., Schwander J., Spahni R., Fischer H. and Stocker T. F. (2012) High-resolution interpolar difference of atmospheric methane around the Last Glacial Maximum. *Biogeosciences* **9**, 3961–3977.

Beck J., Bock M., Schmitt J., Seth B., Blunier T. and Fischer H. (2018) Bipolar carbon and hydrogen isotope constraints of the Holocene methane budget. *Biogeosciences Discussions* **2018**, 1–30.

Biscaye P., Grousset F., Revel M., Van der Gaast S., Zielinski G., Vaars A. and Kukla G. (1997) Asian provenance of glacial dust (Stage 2) in the Greenland Ice Sheet Project 2 ice core, Summit, Greenland. *J Geophys Res-Oceans* **102**, 26765–26781.

Blunier T. and Brook E. J. (2001) Timing of millennial-scale climate change in Antarctica and Greenland during the last glacial period. *Science* **291**, 109–112.

Blunier T., Chappellaz J., Schwander J., Dällenbach A., Stauffer B., Stocker T. F., Raynaud D., Jouzel J., Clausen H. B., Hammer C. U. and Johnsen

S. J. (1998) Asynchrony of Antarctic and Greenland climate change during the last glacial period. *Nature* **394**, 739–743.

Blunier T., Chappellaz J. A., Schwander J., Barnola J. M., Desperts T., Stauffer B. and Raynaud D. (1993) Atmospheric methane, record from a Greenland Ice Core over the last 1000 year. *Geophys Res Lett* **20**, 2219–2222.

Bock M., Schmitt J., Beck J., Seth B., Chappellaz J. and Fischer H. (2017) Glacial/interglacial wetland, biomass burning, and geologic methane emissions constrained by dual stable isotopic CH_4 ice core records. *P Natl Acad Sci USA* **114**, E5778–E5786.

Bock M., Schmitt J., Behrens M., Möller L., Schneider R., Sapart C. and Fischer H. (2010a) A gas chromatography/pyrolysis/isotope ratio mass spectrometry system for high-precision δD measurements of atmospheric methane extracted from ice cores. *Rapid Commun Mass Sp* **24**, 621–633.

Bock M., Schmitt J., Möller L., Spahni R., Blunier T. and Fischer H. (2010b) Hydrogen isotopes preclude marine hydrate CH_4 emissions at the onset of Dansgaard-Oeschger events. *Science* **328**, 1686–1689.

Bory A. J.-M., Biscaye P. E. and Grousset F. E. (2003) Two distinct seasonal Asian source regions for mineral dust deposited in Greenland (NorthGRIP). *Geophys Res Lett* **30**, 1167.

Brook E. J., Harder S., Severinghaus J., Steig E. J. and Sucher C. M. (2000) On the origin and timing of rapid changes in atmospheric methane during the last glacial period. *Global Biogeochel Cy* **14**, 559–572.

Brook E. J., Sowers T. and Orchardo J. (1996) Rapid variations in atmospheric methane concentration during the past 110,000 years. *Science* **273**, 1087–1091.

Buiron D., Stenni B., Chappellaz J., Landais A., Baumgartner M., Bonazza M., Capron E., Frezzotti M., Kageyama M., Lemieux-Dudon B., Masson-Delmotte V., Parrenin F., Schilt A., Selmo E., Severi M., Swingedouw D. and Udisti R. (2012) Regional imprints of millennial variability during the MIS 3 period around antarctica. *Quaternary Science Reviews* **48**, 99–112.

Buizert C., Cuffey K. M., Severinghaus J. P., Baggenstos D., Fudge T. J., Steig E. J., Markle B. R., Winstrup M., Rhodes R. H., Brook E. J., Sowers T. A., Clow G. D., Cheng H., Edwards L. R., Sigl M., McConnell J. R. and Taylor K. C. (2015) The WAIS Divide deep ice core WD2014 chronology – part 1: Methane synchronization (68-31 ka BP) and the gas age-ice age difference. *Clim Past* **11**, 153–173.

Campen R. K., Sowers T. and Alley R. B. (2003) Evidence of microbial consortia metabolizing within a low-latitude mountain glacier. *Geology* **31**, 231–234.

Chappellaz J., Blunier T., Kints S., Dällenbach A., Barnola J. M., Schwander J., Raynaud D. and Stauffer B. (1997) Changes in the atmospheric CH_4 gradient between Greenland and Antarctica during the Holocene. *J Geophys Res-Atmos* **102**, 15987–15997.

Chappellaz J., Stowasser C., Blunier T., Baslev-Clausen D., Brook E. J., Dallmayr R., Faïn X., Lee J. E., Mitchell L. E., Pascual O., Romanini D., Rosen J. and Schüpbach S. (2013) High-resolution glacial and deglacial record of atmospheric methane by continuous-flow and laser spectrometer analysis along the NEEM ice core. *Clim Past* **9**, 2579–2593.

Chappellaz J. A., Fung I. Y. and Thompson A. M. (1993) The atmospheric CH_4 increase since the Last Glacial Maximum. *Tellus B* **45**, 228–241.

Dällenbach A., Blunier T., Flückiger J., Stauffer B., Chappellaz J. and Raynaud D. (2000) Changes in the atmospheric CH_4 gradient between Greenland and Antarctica during the Last Glacial and the transition to the Holocene. *Geophys Res Lett* **27**, 1005–1008.

EPICA Community Members (2006) One-to-one coupling of glacial climate variability in Greenland and Antarctica. *Nature* **444**, 195–198.

Etheridge D. M., Steele L. P., Francey R. J. and Langenfelds R. L. (1998) Atmospheric methane between 1000 A.D. and present: Evidence of anthropogenic emissions and climatic variability. *J Geophys Res* **103**, 15979–15993.

Etheridge D. M., Steele L. P., Langenfelds R. L., Francey R. J., Barnola J. M. and Morgan V. I. (1996) Natural and anthropogenic changes in

atmospheric CO_2 over the last 1000 years from air in Antarctic ice and firn. *J Geophys Res* **101**, 4115–4128.

Etiope G. and Klusman R. W. (2002) Geologic emissions of methane to the atmosphere. *Chemosphere* **49**, 777–789.

Etiope G., Lassey K. R., Klusman R. W. and Boschi E. (2008) Reappraisal of the fossil methane budget and related emission from geologic sources. *Geophys Res Lett* **35**.

Etiope G., Martinelli G., Caracausi A. and Italiano F. (2007) Methane seeps and mud volcanoes in Italy: gas origin, fractionation and emission to the atmosphere. *Geophys Res Lett* **34**.

Fischer H., Behrens M., Bock M., Richter U., Schmitt J., Loulergue L., Chappellaz J., Spahni R., Blunier T., Leuenberger M. and Stocker T. F. (2008) Changing boreal methane sources and constant biomass burning during the last termination. *Nature* **452**, 864–867.

Flückiger J., Blunier T., Stauffer B., Chappellaz M., Spahni R., Kawamura K., Schwander J., Stocker T. F. and Dahl-Jensen D. (2004) N_2O and CH_4 variations during the last glacial epoch: Insight into global processes. *Global Biogeochem Cy* **18**, 1020.

Flückiger J., Dällenbach A., Blunier T., Stauffer B., Stocker T. F., Raynaud D. and Barnola J. M. (1999) Variations in atmospheric N_2O concentration during abrupt climatic changes. *Science* **285**, 227–230.

Flückiger J., Monnin E., Stauffer B., Schwander J., Stocker T. F., Chappellaz J., Raynaud D. and Barnola J. M. (2002) High-resolution holocene N_2O ice core record and its relationship with CH_4 and CO_2. *Global Biogeochem Cy* **16**, 10–1–10–8.

Fourteau K., Faïn X., Martinerie P., Landais A., Ekaykin A. A., Lipenkov V. Y. and Chappellaz J. (2017) Analytical constraints on layered gas trapping and smoothing of atmospheric variability in ice under low-accumulation conditions. *Clim Past* **13**, 1815–1830.

Fraser W. T., Blei E., Fry S. C., Newman M. F., Reay D. S., Smith K. A. and McLeod A. R. (2015) Emission of methane, carbon monoxide, carbon dioxide and short-chain hydrocarbons from vegetation foliage under ultraviolet irradiation. *Plant Cell Environ* **38**, 980–989.

Fung I., John J., Lerner J., Matthews E., Prather M., Steele L. and Fraser P. (1991) Three-dimensional model synthesis of the global methane cycle. *J Geophys Res-Atmos* **96**, 13033–13065.

Grachev A. M., Brook E. J. and Severinghaus J. P. (2007) Abrupt changes in atmospheric methane at the MIS 5b–5a transition. *Geophys Res Lett* **34**, L20703.

Grachev A. M., Brook E. J., Severinghaus J. P. and Pisias N. G. (2009) Relative timing and variability of atmospheric methane and GISP2 oxygen isotopes between 68 and 86 ka. *Global Biogeochem Cy* **23**, 2009.

Hurkuck M., Althoff F., Jungkunst H. F., Jugold A. and Keppler F. (2012) Release of methane from aerobic soil: an indication of a novel chemical natural process? *Chemosphere* **86**, 684–689.

Ji L., Zhang T., Milliken K. L., Qu J. and Zhang X. (2012) Experimental investigation of main controls to methane adsorption in clay-rich rocks. *Appl Geochem* **27**, 2533–2545.

Jouzel J., Stievenard M., Johnsen S. J., Landais A., Masson-Delmotte V., Sveinbjornsdottir A., Vimeux F., Von Grafenstein U. and White J. W. (2007) The GRIP deuterium-excess record. *Quaternary Science Reviews* **26**, 1–17.

Jugold A., Althoff F., Hurkuck M., Greule M., Lenhart K., Lelieveld J. and Keppler F. (2012) Non-microbial methane formation in oxic soils. *Biogeosciences* **9**, 5291–5301.

Kindler P., Guillevic M., Baumgartner M., Schwander J., Landais A. and Leuenberger M. (2014) Temperature reconstruction from 10 to 120 kyr b2k from the NGRIP ice core. *Clim Past* **10**, 887–902.

Kirschke S., Bousquet P., Ciais P., Saunois M., Canadell J. G., Dlugokencky E. J., Bergamaschi P., Bergmann D., Blake D. R., Bruhwiler L., Cameron-Smith P., Castaldi S., Chevallier F., Feng L., Fraser A., Heimann M., Hodson E. L., Houweling S., Josse B., Fraser P. J., Krummel P. B., Lamarque J.-F., Langenfelds R. L., Le Quéré C., Naik V., O'Doherty S., Palmer P. I., Pison I., Plummer D., Poulter B., Prinn R. G., Rigby M., Ringeval B., Santini M., Schmidt M., Shindell D. T., Simpson I. J., Spahni R., Steele L. P.,

Strode S. A., Sudo K., Szopa S., van der Werf G. R., Voulgarakis A., van Weele M., Weiss R. F., Williams J. E. and Zeng G. (2013) Three decades of global methane sources and sinks. *Nature Geoscience* **6**, 813–823.

Landais A., Caillon N., Goujon C., Grachev A. M., Barnola J. M., Chappellaz J., Jouzel J., Masson-Delmotte V. and Leuenberger M. (2004) Quantification of rapid temperature change during DO event 12 and phasing with methane inferred from air isotopic measurements. *Earth Planet Sc Lett* **225**, 221–232.

Lee J., Brook E., Blunier T., Bertler N., Dahl-Jensen D., Severinghaus J., Conway H., Fudge T. and Waddington E. (2018) An 83,000 year old ice core from Roosevelt Island, Ross Sea, Antarctica. *Clim Past Disc* **2018**, 1–44.

Lide D. R. (2004), CRC Handbook of Chemistry and Physics. Vol. 85. CRC press, Boca Raton, FL.

Loulergue L., Schilt A., Spahni R., Masson-Delmotte V., Blunier T., Lemieux B., Barnola J.-M., Raynaud D., Stocker T. F. and Chappellaz J. (2008) Orbital and millennial-scale features of atmospheric CH_4 over the past 800,000 years. *Nature* **453**, 383.

Mayewski P. A., Meeker L. D., Twickler M. S., Whitlow S., Yang Q., Lyons W. B. and Prentice M. (1997) Major features and forcing of high-latitude northern hemisphere atmospheric circulation using a 110,000-year-long glaciochemical series. *J Geophys Res* **102**, 26345–26366.

Mitchell L., Brook E., Lee J. E., Buizert C. and Sowers T. (2013) Constraints on the Late Holocene anthropogenic contribution to the atmospheric methane budget. *Science* **342**, 964–966.

Mitchell L. E., Brook E. J., Sowers T., McConnell J. R. and Taylor K. (2011) Multidecadal variability of atmospheric methane, 1000-1800 C.E. *Journal of Geophysical Research* **116**, G02007.

Mitchell L. E., Buizert C., Brook E. J., Breton D. J., Fegyveresi J., Baggenstos D., Orsi A., Severinghaus J., Alley R. B., Albert M., Rhodes R. H., McConnell J. R., Sigl M., Maselli O., Gregory S. and Ahn J. (2015) Observing and modeling the influence of layering on bubble trapping in polar firn. *J Geophys Res-Atmos* **120**, 2558–2574.

Miteva V., Rinehold K., Sowers T., Sebastian A. and Brenchley J. (2015) Abundance, viability and diversity of the indigenous microbial populations at different depths of the NEEM Greenland ice core. *Polar Res* **34**, 25057.

Miteva V., Sowers T., Schüpbach S., Fischer H. and Brenchley J. (2016) Geochemical and microbiological studies of nitrous oxide variations within the new NEEM Greenland ice core during the last glacial period. *Geomicrobiol J* **33**, 647–660.

Miteva V., Teacher C., Sowers T. and Brenchley J. (2009) Comparison of the microbial diversity at different depths of the GISP2 Greenland ice core in relationship to deposition climates. *Environ Microbiol* **11**, 640–656.

Möller L., Sowers T., Bock M., Spahni R., Behrens M., Schmitt J., Miller H. and Fischer H. (2013) Independent variations of CH_4 emissions and isotopic composition over the past 160,000 years. *Nat Geosci* **6**, 885–890.

NEEM Community Members (2013) Eemian interglacial reconstructed from a Greenland folded ice core. *Nature* **493**, 489–494.

Neftel A., Oeschger H., Schwander J., Stauffer B. and Zumbrunn R. (1982) Ice core sample measurements give atmospheric CO_2 content during the past 40,000 yr. *Nature* **295**, 220–223.

Oxtoby L., Mathis J., Juranek L. and Wooller M. (2016) Estimating stable carbon isotope values of microphytobenthos in the arctic for application to food web studies. *Polar Biol* **39**, 473.

Petit J. R., Jouzel J., Raynaud D., Barkov N. I., Barnola J. M., Basile I., Bender M., Chappellaz J., Davis M., Delaygue G., Delmotte M., Kotlyakov V. M., Legrand M., Lipenkov V. Y., Lorius C., Pepin L., Ritz C., Saltzman E. and Stievenard M. (1999) Climate and atmospheric history of the past 420,000 years from the Vostok ice core, Antarctica. *Nature* **399**, 429–436.

Price P. B. (2000) A habitat for psychrophiles in deep Antarctic ice. *P Natl Acad Sci USA* **97**, 1247–1251.

Price P. B. (2007) Microbial life in glacial ice and implications for a cold origin of life. *FEMS Microbiol Ecol* **59**, 217–231.

1177 Price P. B. and Sowers T. (2004) Temperature dependence of metabolic rates
1178 for microbial growth, maintenance, and survival. *P Natl Acad Sci USA*
1179 **101**, 4631–4636.

1180 Quay P., Stutsman J., Wilbur D., Snover A., Dlugokencky E. and Brown
1181 T. (1999) The isotopic composition of atmospheric methane. *Global Bio-*
1182 *geochem Cy* **13**, 445–461.

1183 Ram M., Donarummo J., Stolz M. R. and Koenig G. (2000) Calibration of
1184 laser-light scattering measurements of dust concentration for Wisconsinan
1185 GISP2 ice using instrumental neutron activation analysis of aluminum-
1186 Results and discussion. *J Geophys Res* **105**, 24.

1187 Ram M. and Koenig G. (1997) Continuous dust concentration profile of pre-
1188 Holocene ice from the Greenland Ice Sheet Project 2 ice core: Dust stadials,
1189 interstadials, and the Eemian. *J Geophys Res-Oceans* **102**, 26641–26648.

1190 Rasmussen S. O., Abbott P. M., Blunier T., Bourne A. J., Brook E., Buchardt
1191 S. L., Buizert C., Chappellaz J., Clausen H. B., Cook E., Dahl-Jensen
1192 D., Davies S. M., Guillevic M., Kipfstuhl S., Laepple T., Seierstad I. K.,
1193 Severinghaus J. P., Steffensen J. P., Stowasser C., Svensson A., Vallelonga
1194 P., Vinther B. M., Wilhelms F. and Winstrup M. (2013) A first chronology
1195 for the North Greenland Eemian Ice Drilling (NEEM) ice core. *Clim Past*
1196 **9**, 2713–2730.

1197 Rasmussen S. O., Bigler M., Blockley S. P., Blunier T., Buchardt S. L.,
1198 Clausen H. B., Cvijanovic I., Dahl-Jensen D., Johnsen S. J., Fischer H.,
1199 Gkinis V., Guillevic M., Hoek W. Z., Lowe J. J., Pedro J. B., Popp T.,
1200 Seierstad I. K., Steffensen J. P., Svensson A. M., Vallelonga P., Vinther
1201 B. M., Walker M. J. C., Wheatley J. J. and Winstrup M. (2014) A strati-
1202 graphic framework for abrupt climatic changes during the Last Glacial Pe-
1203 riod based on three synchronized Greenland ice-core records: refining and
1204 extending the INTIMATE event stratigraphy. *Quaternary Sci Rev* **106**,
1205 14–28.

1206 Rhodes R. H., Brook E. J., Chiang J. C., Blunier T., Maselli O. J., Mc-
1207 Connell J. R., Romanini D. and Severinghaus J. P. (2015) Enhanced trop-
1208 ical methane production in response to iceberg discharge in the North
1209 Atlantic. *Science* **348**, 1016–1019.

Rhodes R. H., Brook E. J., McConnell J. R., Blunier T., Sime L. C., Faïn X. and Mulvaney R. (2017) Atmospheric methane variability: Centennial-scale signals in the Last Glacial Period. *Global Biogeochem Cy* **31**, 575–590.

Rhodes R. H., Faïn X., Brook E. J., McConnell J. R., Maselli O. J., Sigl M., Edwards J., Buizert C., Blunier T., Chappellaz J. and Freitag J. (2016) Local artifacts in ice core methane records caused by layered bubble trapping and in situ production: a multi-site investigation. *Clim Past* **12**, 1061–1077.

Rhodes R. H., Faïn X., Stowasser C., Blunier T., Chappellaz J., McConnell J. R., Romanini D., Mitchell L. E. and Brook E. J. (2013) Continuous methane measurements from a late Holocene Greenland ice core: Atmospheric and in-situ signals. *Earth Planet Sc Lett* **368**, 9–19.

Rohde R. A., Price P. B., Bay R. C. and Bramall N. E. (2008) In situ microbial metabolism as a cause of gas anomalies in ice. *P Natl Acad Sci USA* **105**, 8667–8672.

Rosen J. L., Brook E. J., Severinghaus J. P., Blunier T., Mitchell L. E., Lee J. E., Edwards J. S. and Gkinis V. (2014) An ice core record of near-synchronous global climate changes at the Bolling transition. *Nat Geosci* **7**, 459–463.

Saltzman E. S., Aydin M., Williams M. B., Verhulst K. R. and Gun B. (2009) Methyl chloride in a deep ice core from Siple Dome, Antarctica. *Geophys Res Lett* **36**, L03822.

Sapart C. J., van der Veen C., Vigano I., Brass M., van de Wal R. S. W., Bock M., Fischer H., Sowers T., Buizert C., Sperlich P., Blunier T., Behrens M., Schmitt J., Seth B. and Röckmann T. (2011) Simultaneous stable isotope analysis of methane and nitrous oxide on ice core samples. *Atmos Meas Tech* **4**, 2607–2618.

Saunois M., Bousquet P., Poulter B., Peregon A., Ciais P., Canadell J. G., Dlugokencky E. J., Etiope G., Bastviken D., Houweling S. and et al. (2016) The global methane budget 2000–2012. *Earth System Science Data* **8**, 697–751.

Schilt A., Baumgartner M., Schwander J., Buiron D., Capron E., Chappellaz J., Loulergue L., Schüpbach S., Spahni R., Fischer H. and Stocker T. F. (2010) Atmospheric nitrous oxide during the last 140,000 years. *Earth Planet Sc Lett* **300**, 33–43.

Schmitt J., Schneider R. and Fischer H. (2011) A sublimation technique for high-precision measurements of $\delta^{13}CO_2$ and mixing ratios of CO_2 and N_2O from air trapped in ice cores. *Atmos Meas Tech* **4**, 1445–1461.

Schmitt J., Seth B., Bock M. and Fischer H. (2014) Online technique for isotope and mixing ratios of CH_4, N_2O, Xe and mixing ratios of organic trace gases on a single ice core sample. *Atmos Meas Tech* **7**, 2645–2665.

Schüpbach S., Fischer H., Bigler M., Erhardt T., Gfeller G., Leuenberger D., Mini O., Mulvaney R., Abram N. J., Fleet L., Frey M. M., Thomas E., Svensson A., Dahl-Jensen D., Kettner E., Kjaer H., Seierstad I., Steffensen J. P., Rasmussen S. O., Vallelonga P., Winstrup M., Wegner A., Twarloh B., Wolff K., Schmidt K., Goto-Azuma K., Kuramoto T., Hirabayashi M., Uetake J., Zheng J., Bourgeois J., Fisher D., Zhiheng D., Xiao C., Legrand M., Spolaor A., Gabrieli j., Barbante C., Kang J.-H., Hur S. D., Hong S. B., Hwang H. J., Hong S., Hansson M., Iizuka Y., Oyabu I., Muscheler R., Adolphi F., Maselli O., McConnell J. and Wolff E. W. (2018) Greenland records of aerosol source and atmospheric lifetime changes from the Eemian to the Holocene. *Nat Comm* **9**, 1476.

Schwander J. and Stauffer B. (1984) Age difference between polar ice and the air trapped in its bubbles. *Nature* **311**, 45–47.

Smith H., Wahlen M., Mastroianni D., Taylor K. and Mayewski P. A. (1997) The CO_2 concentration of air trapped in Greenland Ice Sheet Project 2 ice formed during periods of rapid climate change. *J Geophys Res-Oceans* **102**, 26–577.

Snover A. K., Quay P. D. and Hao W. M. (2000) The D/H content of methane emitted from biomass burning. *Global Biogeochem Cy* **14**, 11–24.

Souchez R., Lemmens M. and Chappellaz J. (1995) Flow-induced mixing in the GRIP basal ice deduced from the CO_2 and CH_4 records. *Geophys Res Lett* **22**, 41–44.

Sowers T. (2001) N_2O record spanning the penultimate deglaciation from the Vostok ice core. *J Geophys Res-Atmos* **106**, 31903–31914.

Sowers T. (2006) Late quaternary atmospheric CH_4 isotope record suggests marine clathrates are stable. *Science* **311**, 838–840.

Sowers T. (2010) Atmospheric methane isotope records covering the Holocene period. *Quaternary Sci Rev* **29**, 213–221.

Stauffer B., Flückiger J., Monnin E., Nakazawa T. and Aoki S. (2003) Discussion of the reliability of CO_2, CH_4 and N_2O records from polar ice cores. *Mem Natl Inst Polar Res* **57**, 139–152.

Steffensen J. P. (1997) The size distribution of microparticles from selected segments of the Greenland Ice Core Project ice core representing different climatic periods. *J Geophys Res* **102**, 26755–26763.

Stowasser C., Buizert C., Gkinis V., Chappellaz J., Schüpbach S., Bigler M., Faïn X., Sperlich P., Baumgartner M., Schilt A. and Blunier T. (2012) Continuous measurements of methane mixing ratios from ice cores. *Atmos Meas Tech* **5**, 999–1013.

Svensson A., Biscaye P. E. and Grousset F. E. (2000) Characterization of late glacial continental dust in the Greenland Ice Core Project ice core. *J Geophys Res-Atmos* **105**, 4637–4656.

Thompson A. M., Chappellaz J. A. and Fung I. Y. (1993) The atmospheric CH_4 increase since the Last Glacial Maximum. *Tellus B* **45**, 228–241.

Tung H., Price P., Bramall N. and Vrdoljak G. (2006) Microorganisms metabolizing on clay grains in 3-km-deep Greenland basal ice. *Astrobiology* **6**, 69–86.

Tung H. C., Bramall N. E. and Price P. B. (2005) Microbial origin of excess methane in glacial ice and implications for life on Mars. *P Natl Acad Sci USA* **102**, 18292–18296.

Újvári G., Stevens T., Svensson A., Klötzli U. S., Manning C., Németh T., Kovács J., Sweeney M. R., Gocke M., Wiesenberg G. L., Markovic S. B. and Zech M. (2015) Two possible source regions for central Greenland last glacial dust. *Geophys Res Lett* **42**.

Umezawa T., Brenninkmeijer C. A., Röckmann T., van der Veen C., Tyler S. C., Fujita R., Morimoto S., Aoki S., Sowers T., Schmitt J., Bock M., Beck J., Fischer H., Michel S. E., Vaughn B. H., Miller J. B., White J. W. C., Brailsford G., Schaefer H., Sperlich P., Brand W. A., Rothe M., Blunier T., Lowry D., Fisher R. E., Nisbet E. G., Rice A. L., Bergamaschi P., Veidt C. and Levin I. (2018) Interlaboratory comparison of δ^{13}C and δ D measurements of atmospheric CH_4 for combined use of data sets from different laboratories. *Atmos Meas Tech* **11**, 1207.

Wang B., Lerdau M. and He Y. (2017) Widespread production of nonmicrobial greenhouse gases in soils. *Global Change Biology* **23**, 4472–4482.

Whiticar M. and Schaefer H. (2007) Constraining past global tropospheric methane budgets with carbon and hydrogen isotope ratios in ice. *Philos T Roy Soc A* **365**, 1793–1828.

York D., Evensen N. M., Martınez M. L. and De Basabe Delgado J. (2004) Unified equations for the slope, intercept, and standard errors of the best straight line. *Am J Phys* **72**, 367–375.